END
DATE
FILMED

DTIC

1.0

2.8   2.5

3.2   2.2

3.6

1.1   4.0   2.0

1.8

1.25   1.4   1.6

MICROCOPY RESOLUTION TEST CHART
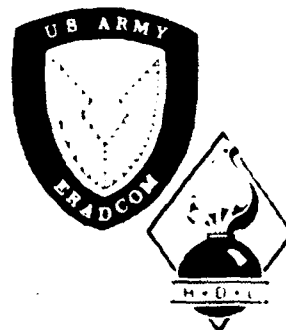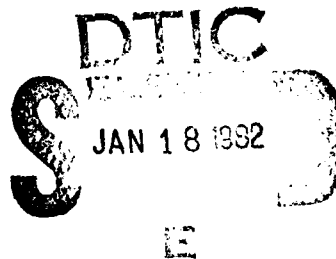
NATIONAL BUREAU OF STANDARDS

AD A109715

LEVEL II (12)

HDL-CR-81-288-1
August 1981

FINAL REPORT: DUAL-CHANNEL FUEL CONTROL PROGRAM
PHASE II

by John Itamoto

DTIC
JAN 18 1992
E

Prepared by
Garrett Pneumatic Systems Division
of The Garrett Corporation
111 South 34th Street
Phoenix, AZ 85010

U.S. Army Electronic Research
and Development Command
Harry Diamond Laboratories
Adelphi, MD 20783

DTIC FILE COPY

Approved for public release; distribution unlimited

SECURITY CLASSIFICATION OF THIS PAGE (When Data Entered)

REPORT DOCUMENTATION PAGE		READ INSTRUCTIONS BEFORE COMPLETING FORM
1. REPORT NUMBER HDL - CR-81-288-1	2. GOVT ACCESSION NO. AD-A109 915	3. RECIPIENT'S CATALOG NUMBER
4. TITLE (and Subtitle) Dual-Channel Fuel Control Program		5. TYPE OF REPORT & PERIOD COVERED Final Report for Period 4-1978 to 8-1980
		6. PERFORMING ORG. REPORT NUMBER 41-2710A
7. AUTHOR(s) John Itamoto (Contract Monitor: John Goto, Harry Diamond Laboratories)		8. CONTRACT OR GRANT NUMBER(s) N00019-78-G-0288 TASK 7813
9. PERFORMING ORGANIZATION NAME AND ADDRESS Garrett Pneumatic Systems Division 111 South 34 Street Phoenix, AZ, 85010		10. PROGRAM ELEMENT, PROJECT, TASK AREA & WORK UNIT NUMBERS
11. CONTROLLING OFFICE NAME AND ADDRESS Harry Diamond Laboratories 2800 Powder Mill road Adelphi, MD 20783		12. REPORT DATE August 1981
		13. NUMBER OF PAGES 80
14. MONITORING AGENCY NAME & ADDRESS(if different from Controlling Office)		15. SECURITY CLASS. (of this report) Unclassified
		15a. DECLASSIFICATION/DOWNGRADING SCHEDULE

16. DISTRIBUTION STATEMENT (of this Report)

Approved for public release; distribution unlimited

17. DISTRIBUTION STATEMENT (of the abstract entered in Block 20, if different from Report)

18. SUPPLEMENTARY NOTES

DCASMA Code: S0302A
AMCMS Code: 612120H250011
DCASR Code: S4403A

19. KEY WORDS (Continue on reverse side if necessary and identify by block number)

Fluidic
Fuel Control
Control System

20. ABSTRACT (Continue on reverse side if necessary and identify by block number)

This report presents the results of a program conducted by Garrett to investigate a dual-channel fuel control for gas turbine engines which could be used in military ground vehicles. The program presents a control system with requirements that are deemed necessary to provide a military

DD FORM 1473 EDITION OF 1 NOV 65 IS OBSOLETE

1   UNCLASSIFIED

SECURITY CLASSIFICATION OF THIS PAGE (When Data Entered)

gas turbine-powered vehicle with battlefield survivability and minimal restriction on the capability of completing the vehicle mission.

This study showed that a parallel dissimilar technology backup control was the desirable approach and that fluidics was the ideal technology to perform this function due to its low cost, reliability, immunity to radiation, and ability to perform computation and logic commensurate with the requirements of achieving mission completion with no degradation in the vehicle's battlefield survivability.

FOREWORD

This is the final report of a program conducted by Garrett Pneumatic Systems Division of The Garrett Corporation (formerly AiResearch Manufacturing Company of Arizona). The purpose of this program was to develop a dual-channel electrical and fluidic fuel control for application on typical military automotive gas turbine engines. This is the second phase of the program and is devoted to the development of critical fluidic computational and control mode switching logic circuits.

The program was authorized by the Naval Air Systems Command under Contract N00019-78-G-0288 and was monitored by Mr. John Goto of Harry Diamond Laboratories of the Department of the Army. The program was conducted from April, 1978, to August, 1980.

Publication of this report does not constitute approval by any member of the Department of Defense of the findings or conclusions contained herein.

Accession For

NTIS
I
U
J

Dist

A

3

CONTENTS

FIGURES

5

CONTENTS (cont'd)

CONTENTS (cont'd)

CONTENTS (cont'd)

1. INTRODUCTION

This is the final report of Phase II of a program conducted by Garrett Pneumatic Systems Division (formerly AiResearch Manufacturing Company of Arizona) to develop the fluidic portion of a dual-channel fuel control. The control is intended for use on a military gas turbine engine such as the ITI-GT601 engine. The primary objective of the program was to obtain a control system with two complete and parallel modes of control represented by dissimilar technologies. To this end, the primary controller is electronic and the secondary controller is fluidic.

The tasks to be performed in this phase of the program were:

1. Preparation of a preliminary packaging/installation layout for all fluidic sensors and interface components.

2. Analysis and design of an engine speed sensor which would meet engine performance. Fabrication and laboratory testing of the speed sensor, emphasizing acceleration/deceleration and overspeed control.

3. Development of critical fluidic computational and control mode switching logic circuits, including fabrication and laboratory test.

1.1 Background

The dual-channel fuel control concept is seen as a means of increasing the survivability of combat vehicles in battle conditions. Presently, controls on some military gas turbines provide only a marginal "limp-home" backup mode in the event that the primary controller (electronic) fails and the capability of restart is also lost.

In Phase I of this program (the results of which were presented in Report HDL-CR-78-186-1), it was determined that the dual-channel fuel control concept was feasible. The ITI-GT601 gas turbine was used as a model. Beyond the conventional fuel control parameters used with gas turbine engines, the GT601 engine has a variable turbine nozzle (VTN) system and a recuperator (stationary) heat exchanger

which increase the required control parameters for this engine. Figure 1 depicts a schematic diagram of a typical military gas turbine engine. A block diagram of the dual-channel concept developed for this program using fluidic technology is shown in Figure 2.

1.2 Summary

This phase of the Dual-Channel Fuel Control Development Program addressed the evolution and development of fluidic circuits to accomplish the following:

1. Detect an electronic fuel control failure condition.

2. Execute a control mode selection.

3. Switch from the primary electronic control mode to the fluidic mode in sufficient time to prevent engine failure. The failure modes evaluated were those which were beyond the capability of manual switchover.

A preliminary analysis of the ITI-GT601 engine was made to assess the feasibility of installation of redundant sensors for fluidic controls. Upon satisfactory conclusion of this feasibility study, further interface design was left for sensor design in Phase III.

The major work effort for Phase II consisted of two parts which are shown diagramatically in Figure 3. Part One addressed the analysis and design of the critical switching circuits and interface schemes. In Part Two, the critical sensing components [gas generator turbine inlet temperature (T_4) and gas generator speed (N_{GG})] and switching circuits were fabricated and tested. The present temperature sensor for the GT601 engine is a fluidic oscillator with an electrical output. For this program, the direct fluidic frequency output of the oscillator was used. Performance simulations were conducted using a pseudo-temperature test rig.

Numerous speed sensor concepts were evaluated and tested for the Mobility Equipment Research and Development Command[1]. The digital-type speed sensor (chopper) with a

_____

[1] Mobility Equipment Research and Development Command, Final Report DAAK70-78-C-0093.

10

GAS GENERATOR POWER TURBINE

INLET 1

N_{GG}

N_{PT}

TRANSMISSION

N_{GG} GAS GENERATOR SPEED

T_G GAS GENERATOR TURBINE

HEAT EXCHANGER

EXHAUST

STATION NO.

1. INLET
2. COMPRESSOR C_1
3. COMPRESSOR C_2
3.5 COMBUSTOR INLET
4. T_G INLET
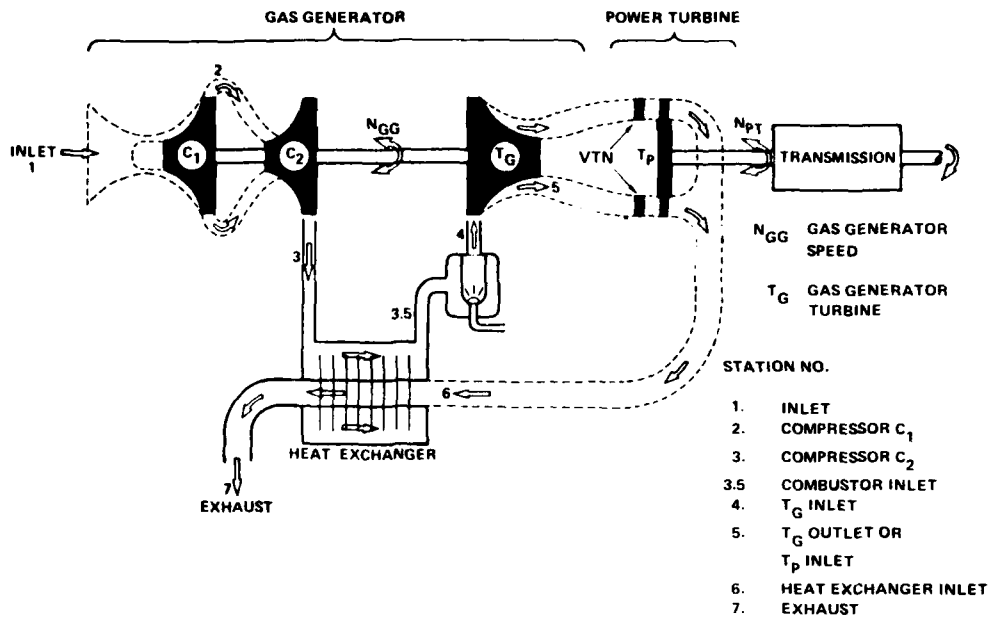5. T_G OUTLET OR T_P INLET
6. HEAT EXCHANGER INLET
7. EXHAUST

Figure 1. Schematic diagram of typical military automotive gas turbine engine.
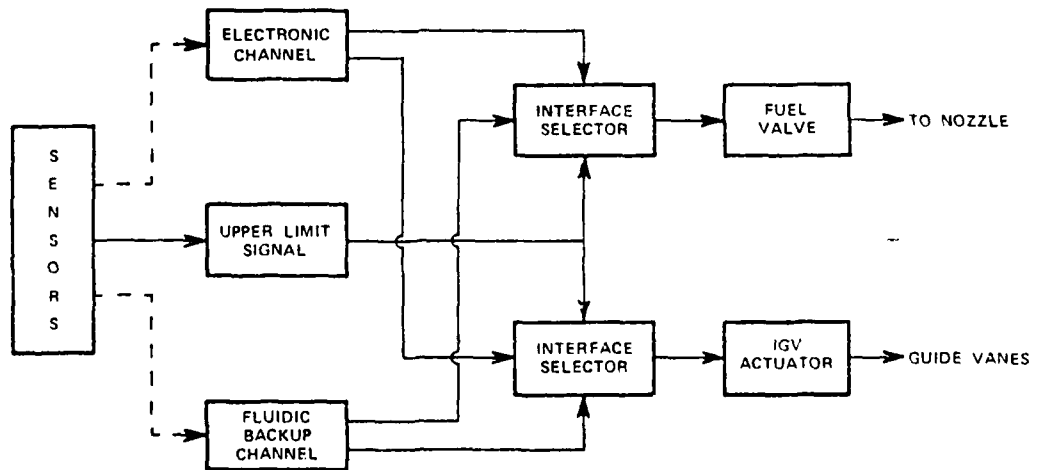
Figure 2. Block diagram of dual-channel fuel control.

11

PART 1
ANALYSIS

PART 2
FABRICATION AND TESTING

STUDY
FAILURE MODES AND CRITICALITY ANALYSIS OF GT601

DETERMINE
CRITICAL ENGINE PARAMETERS

STUDY
RELATED ENGINE COMPONENTS

SIMPLIFY
EXISTING ENGINE MODEL

COMPARE
DYNAMIC BEHAVIOUR OF THESE COMPONENTS TO THE RESPONSIVENESS OF FLUIDIC COMPONENTS USED TO SENSE PARAMETERS

COLLECT
DYNAMIC INFORMATION ON ENGINE, FLUIDIC SENSING COMPONENTS, AND FAILURE BEHAVIOUR OF ENGINE PARAMETERS

DETERMINE
PARAMETERS WITH WORST MARGIN BETWEEN EVENT AND EVENT AS SENSED

SIMULATE
ENGINE WITH FLUIDIC FAILURE DETECT CIRCUITS UNDER CRITICAL FAILURE CONDITIONS

CAN A SWITCH OF CONTROL MODES BE SAFELY EXECUTED AFTER A CRITICAL FAILURE?

−

+

DESIGN
INTERFACE WITH NO POSITIVE FAILURE MODES

GO TO PART 2

DEVELOP SENSING COMPONENTS FOR THE MOST CRITICAL PARAMETER(S)

SET UP TEST HARDWARE IN A CONFIGURATION REPRESENTATIVE OF HOW IT IS TO BE USED ON ENGINE

CONDUCT FREQUENCY RESPONSE TEST OF FLUIDIC COMPONENTS

RUN SIMULATIONS OF FAILURE CONDITION AND MONITOR CIRCUIT RESPONSE

INSIGHTS
INVESTIGATION OF OTHER SENSOR POSSIBILITIES

SUGGESTIONS OF IMPROVEMENTS
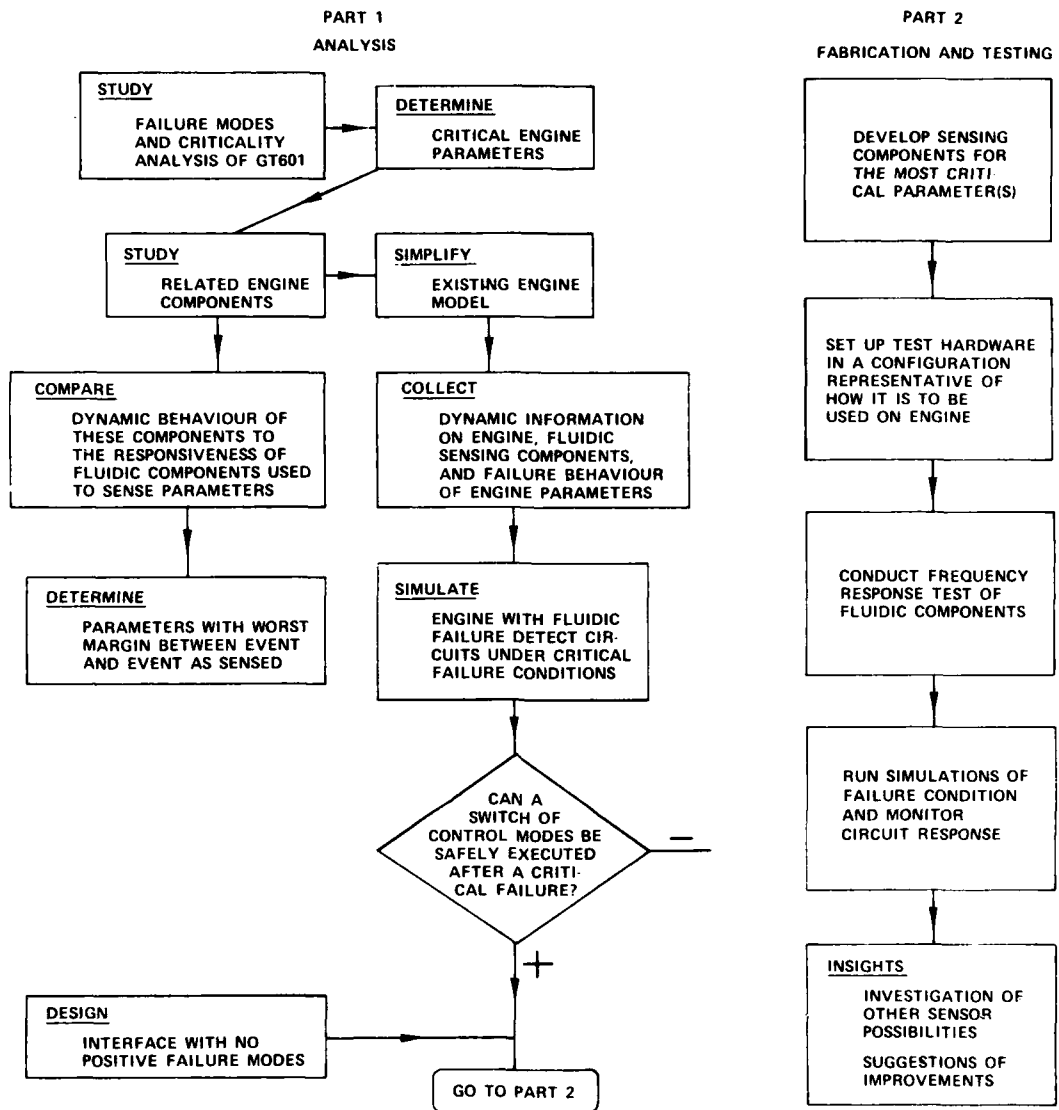
Figure 3.   Failure detection circuit analysis diagram.

12

frequency-to-analog converter was evaluated; however, the laminar amplifier disc speed sensor described in Reference 1 was considered to have the greatest potential for success in this application. This sensor was evaluated and tested for this application and will be further developed in Phase III.

2. TECHNICAL DISCUSSION

2.1 Analysis

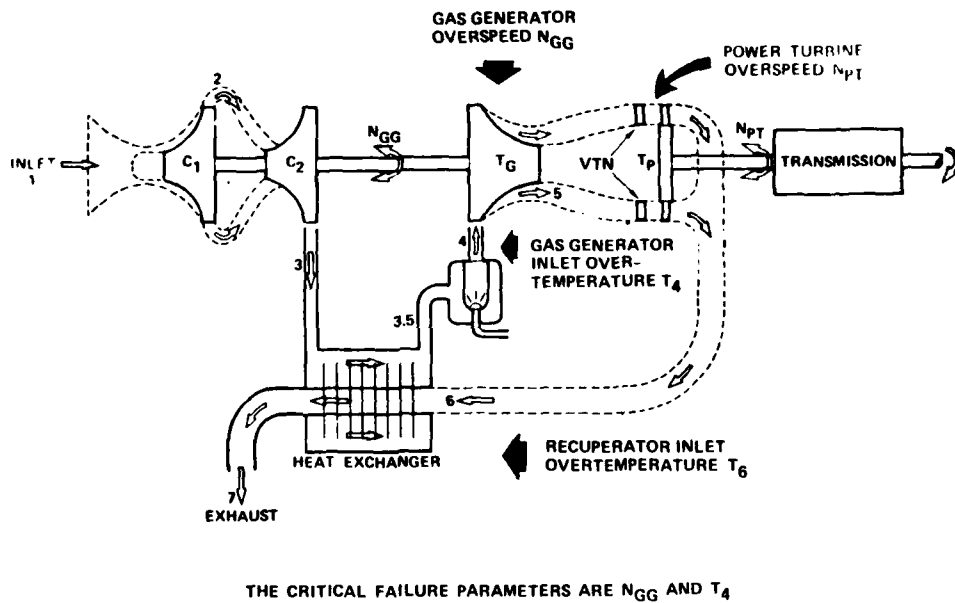Figure 4 represents a typical automatic gas turbine engine.

THE CRITICAL FAILURE PARAMETERS ARE N_{GG} AND T_4

Figure 4. Typical automotive gas turbine engine.

13

Of all the components of a gas turbine engine, the combustor is by far the swiftest to convert input to output. The fuel residence time of a typical combustor is less than 10 milliseconds. Since the engine controls govern fuel flow rate and the variable turbine nozzles, the engine parameters which require monitoring are those immediately affected by the combustor as listed below.

Gas generator inlet temperature T_4

Recuperator inlet temperature T_6

Gas generator speed N_{GG}

Power turbine speed N_{PT}

Failure conditions are overtemperature and overspeed.

A comparison of the time constants related to the components which generate the parameters and the time constants of the sensors used to sense the parameters show that the T_4 and N_{GG} parameters associated with the gas generator are the most critical.

TABLE I. COMPONENT AND SENSOR TIME CONSTANTS

Component	Component Time Constant	Sensor Time Constant
Combustor (temperature)	Six milliseconds fuel residence time	Fluidic Temperature Sensor $\tau = 0.7$ s at 100 percent N_{GG} $\tau = 2.5$ s at 50 percent N_{GG}
Gas Generator and Power Turbine Wheels (speed)	1 s	Fluidic Speed Sensor $\tau = 0.1$ s
Recuperator (temperature)	15 to 19 s	Fluidic Temperature Sensor $\tau = 0.7$ s at maximum temperature set point

An overspeed condition of the gas generator (N_{GG}) can be sensed and corrected by a fluidic speed sensor. However, this condition will be considered because of its close relationship to changes in fuel flow and also to obtain a better understanding of noise suppression and the manner in which this affects the response characteristics of the speed sensor.

The power turbine speed parameter (N_{PT}) is further removed from changes in fuel command and is also provided with a measure of safety by the variable turbine nozzle (VTN). Thus, the situation of sensing and providing an appropriate corrective action for a gas turbine inlet over-temperature condition (T_4) is by far the most demanding task for the fuel control system.

In the event there is a failure in which an increase in fuel flow is commanded, the gas turbine inlet overtemperature condition (T_4) should lead all other criti-cal overtemperatures and overspeed conditions and thus should be used for sensing and providing correction.

The failure circuits for T_4, T_6, and the circuits for N_{GG} and N_{PT} should be the same (see Figure 5).
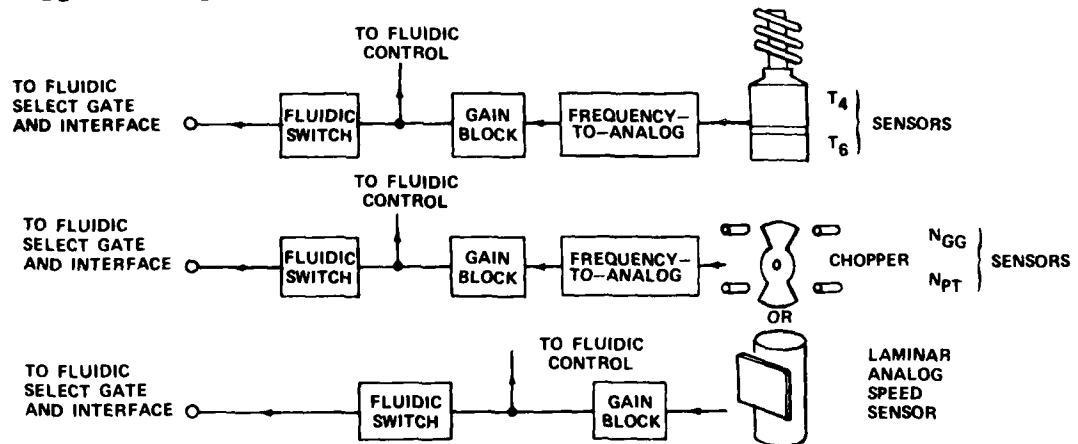

Figure 5. Block diagram of sensor-to-fluidic switchover logic.

A model simulation is presented in the following para-graphs. For purposes of reconstruction of the simulation, a more detailed presentation is included in Appendix A.
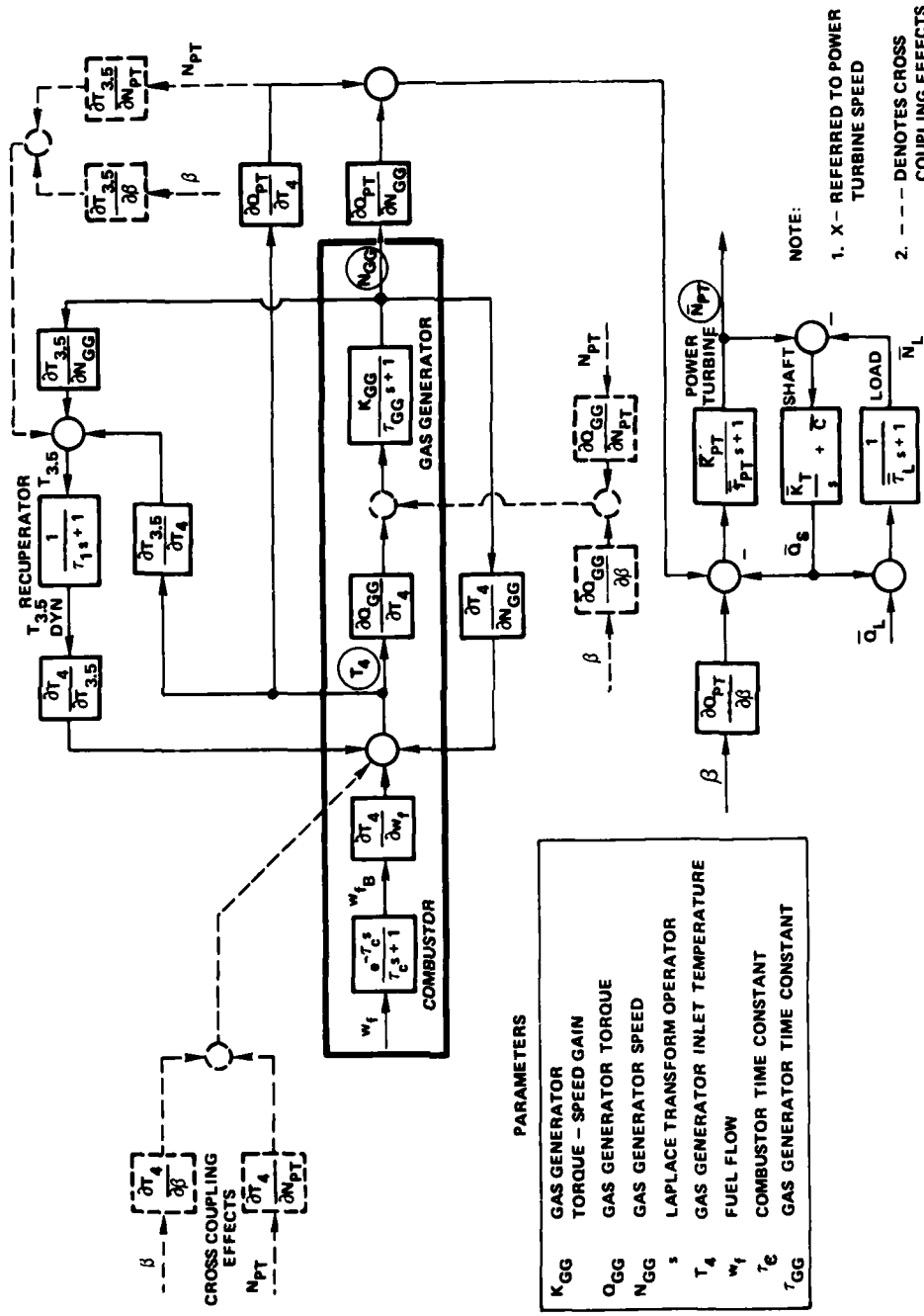
15

2.2 Model Simulation

The block diagram shown in Figure 6 is a linearized model of the GT601 engine and driveline. In conducting the overtemperature and overspeed simulations, the portion of the model heavily outlined in Figure 6 was used. The engine parameters outside the box affect T_4 and N_{GG}; but for typical fuel command changes, their contributions are negligible for about 500 milliseconds. The failure conditions are expected to occur within the 500-millisecond time frame and, therefore, the truncated model is sufficient for extracting meaningful information.

Failure conditions were represented by changes in T_4 and N_{GG} in which excursions from maximum levels of operation to failure levels are linear ramps. The rates of $\dot{T}_4$ and $\dot{N}_{GG}$ due to fuel command changes on the VTN were converted into equivalent changes of fuel flow. The failures would occur in the electronic channel. When the failure signals reached the level of the switch points, the fluidic control would then dictate the command signal before failure (Figures 7 and 8). Noise inputs applied to the failure signals were simulated T_4 and N_{GG} signals. These signals were used to determine the effects of noise on switching.

2.3 Temperature Simulation

Temperature simulations were conducted by making the speed signal path switch inactive. The model initially begins operating at a high control temperature (T_4 = 1800F) and a $\dfrac{\partial w_f}{\partial t}$ change is commanded to give a T_4 change at a given rate. Known dynamic information is used for the fluidic components. The engine parameters change as a function of operating point (N_{GG}, T_4, etc.); however, in these simulations, they were assumed to be constant. The various partial derivatives were checked for drastic changes when the T_4 level increased from 1800F to 2000F. The changes were found to be small; thus, the assumption of constant values would be sufficient and reasonable for purposes of this simulation.
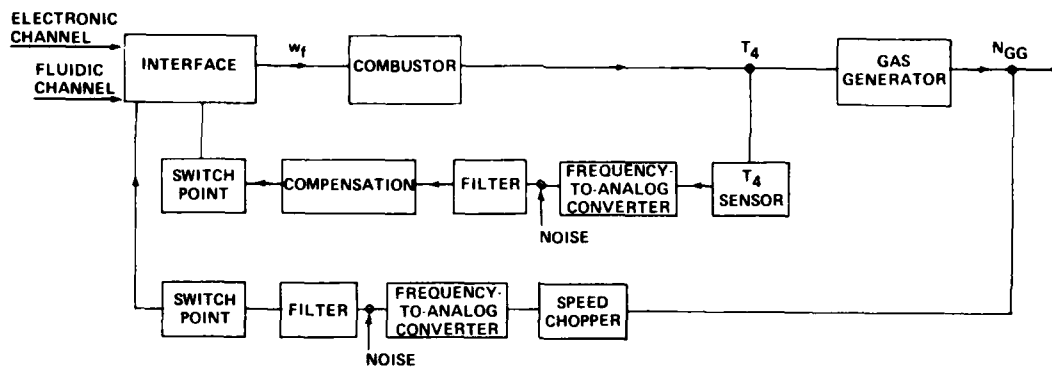
16

Figure 6. Linearized model of GT601.

43ART00151

NOTE:

1. x — REFERRED TO POWER
   TURBINE SPEED

2. – – – DENOTES CROSS
        COUPLING EFFECTS

PARAMETERS

K_{GG} GAS GENERATOR
            TORQUE – SPEED GAIN

Q_{GG} GAS GENERATOR TORQUE

N_{GG} GAS GENERATOR SPEED

s LAPLACE TRANSFORM OPERATOR

T_4 GAS GENERATOR INLET TEMPERATURE

w_f FUEL FLOW

τ_c COMBUSTOR TIME CONSTANT

τ_{GG} GAS GENERATOR TIME CONSTANT

17

Figure 7. Block diagram of computer model of
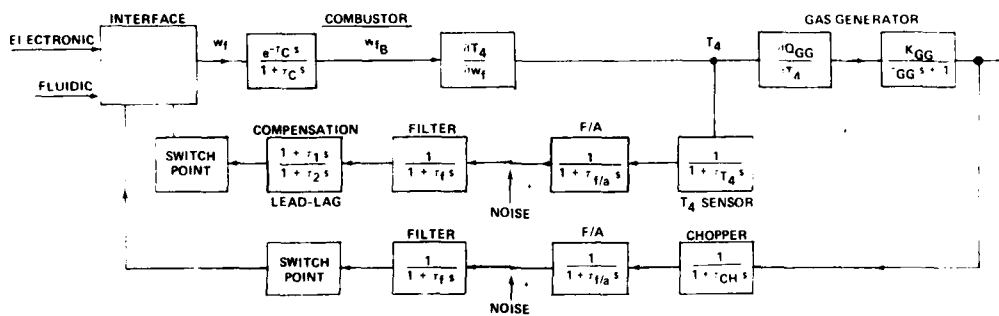engine and failure detection circuits.

Figure 8. Simplified dynamic model.

18

Table II shows the range of values of the fluidic components and engine parameters used in the simulations.

TABLE II.   FLUIDIC CONTROL CHANNEL ANALYTICAL
SIMULATION PARAMETERS

Fluidic Components and Engine Parameters	Range of Values
$\dfrac{\partial T_4}{\partial w_f}$	2 to 13F per lbm per hr
S - switch and interface delay	10 to 30 milliseconds
τ_C - combustor fuel residence time	6 milliseconds
τ_{T_4} - T_4 sensor time constant	0.7 to 2.5 seconds
$\tau_{f/a}$ - frequency-to-analog conversion time constant	20 to 30 milliseconds
w_f - fuel flow	200 lbm per hr maximum
τ_f - filter time constant	zero to 0.025 second
Lead/lag ratio	1, 3, and 10
$\dot{T}_4$ - temperature rates	200 to 1000F per seconds

Figures 9 and 10 are plots of T_4 and T_4-sensor versus time. They show that an overtemperature circuit with a 2.5-second T_4 sensor, a compensator with a lead-lag ratio of 3, and a noise filter set at 0.005 and 0.025 second, can respond adequately to $\dot{T}_4$ values much higher than seen in normal engine operation. (In the case of the plots, $\dot{T}_4$ = 700 degrees per second.) The filter and switch point are boot-strapped. Increasing the size of the filter necessitates use of a lower switchpoint. The tradeoff is not even since the filter may affect response more than it attenuates noise.
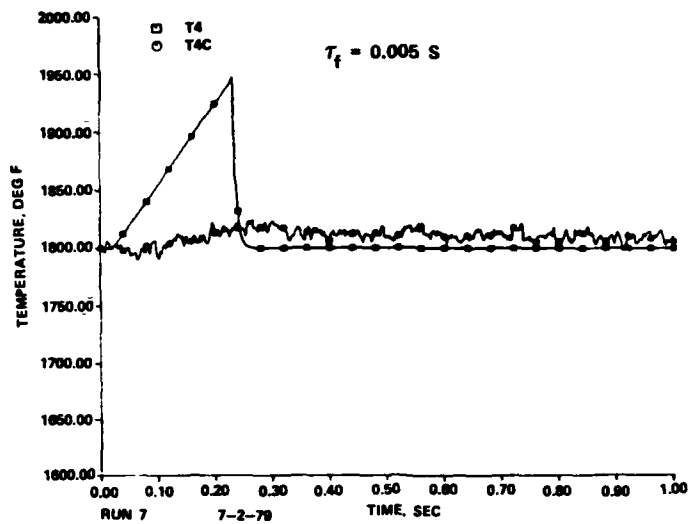
19

Figure 9. T_4 and sensed T_4 signals with
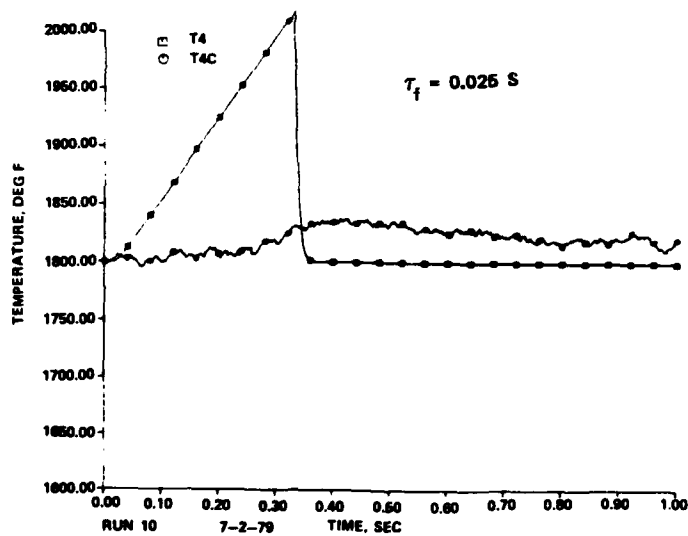high frequency filter (simulated).

Figure 10. T_4 and sensed T_4 signals with
low frequency filter (simulated).

20

Using a fluidic failure circuit made of state-of-the-art components is dynamically adequate within the limits of this analysis.

2.4 Speed Simulation

The time constants of the gas generator and power turbine are larger than the time constants of the speed sensors used to sense their speeds. Changes in speed would not occur as quickly as those in temperature; therefore, there is no concern about the dynamic ability of fluidic speed sensors to respond to overspeed conditions. The speed circuit used to a chopper-type frequency-to-analog converter which is slowest (relatively) to respond. The model used is as shown in Figure 8 with the temperture path switch shorted. Thus, an overtemperature condition does not trigger the interface before an overspeed condition can develop (see Figure 11).
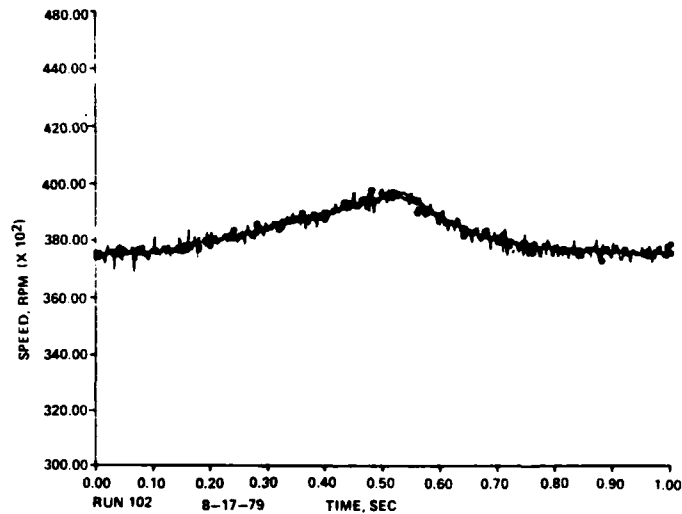

Figure 11. Speed and sensed speed without filter (simulated).

21

Figure 12 is a plot of the gas generator simulated speed and the sensed speed. The speed is initially at the highest control level. The computer then inputs a command to the maximum fuel flow rate. The noise seen is that of the speed sensors and the frequency-to-analog converter. As anticipated, it is evident that the sensed signal follows quite well.
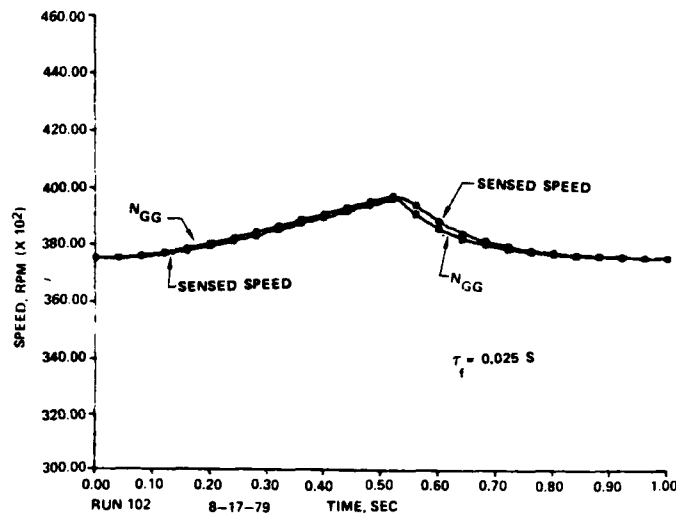

Figure 12. Speed and sensed speed with filter (simulated).

Figure 12 also shows a speed simulation with a high frequency filter greater than a decade out from the speed sensor frequency. The sensed speed lags less than 10 milliseconds during the speed ramp and 20 milliseconds less when fuel is cut back and the speed drops. The response rate is sufficiently high to permit enhancing the signal quality at some loss of response should that become desirable.

22

Figure 13 shows a simulation conducted with simultan-
eously active speed and temperature failure signal paths.
This is similar to the overtemperature plots and confirms
the expectation that, with a sudden increase in fuel com-
mand, an overtemperature condition would occur before over-
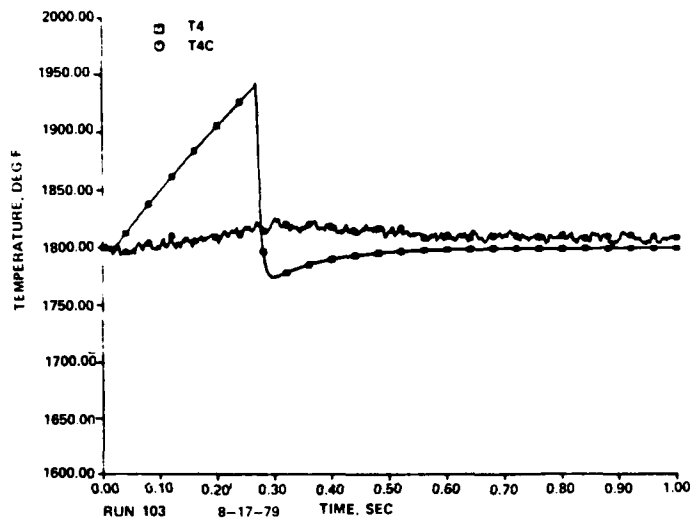speed occurs.

Figure 13.   Simulated T_4 and sensed T_4
with effects of speed.

The model did not have the feedback effects on T_4 due
to the gas generator speed ($\frac{\partial T_4}{\partial N_{GG}}$ is negative).   In reality,
as the speed of the turbine increases, the model would begin
to attenuate the overtemperature condition.   The analysis
shows that the control system is safe with considerable mar-
gin.

23

2.5 Interface

If the electronic control channel fails, the fluidic channel must be allowed to control the fuel metering valve and variable turbine nozzle actuator. This must be accomplished through an interface which must also accept electronic and manual switch signals. Various block diagrams of configurations implementing the switchover from electronic to fluidic control are shown in Figures 14 through 17. The configurations were evaluated with respect to the following considerations:

1. The interface must have no positive failure modes. A failure in the interface must leave at least one control channel open.

2. The switchover must be mutually exclusive. Erroneous information from the failed controller must not be capable of influencing the secondary channel.

3. The number of times the weakest components are cycled during normal operation should be minimized.

4. Time delays in generating a control signal should be minimized.

2.5.1 Type 1 Configuration

In Figure 14, the failure of the summing amplifier eliminates both channels of information. In the shunt approach, the shunt must be complete or an erroneous control signal will develop.

2.5.2 Type 2 Configuration

In Figure 15, the failure of the summing amplifier leaves the interface free of positive failure modes; however, a transient delay related to activating the fluidic supply exists.
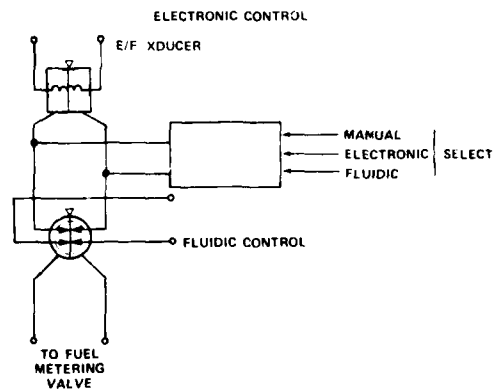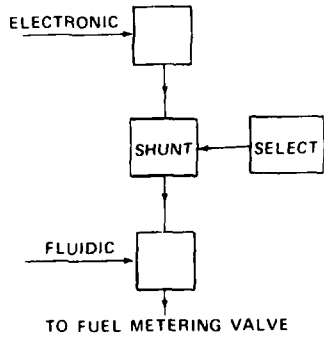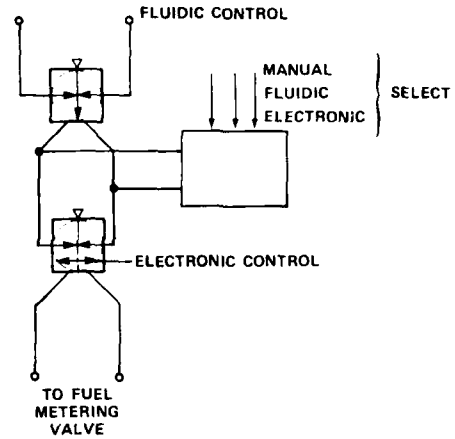
24
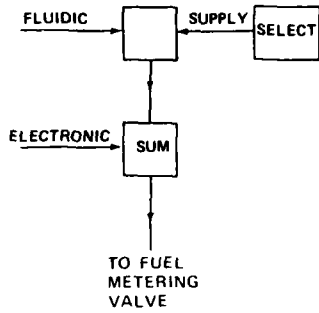
BLOCK DIAGRAM

IMPLEMENTATION

Figure 14. Signal channel supply or signal shunt select (Type 1).

25

BLOCK DIAGRAM

IMPLEMENTATION
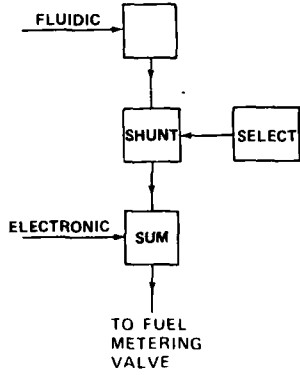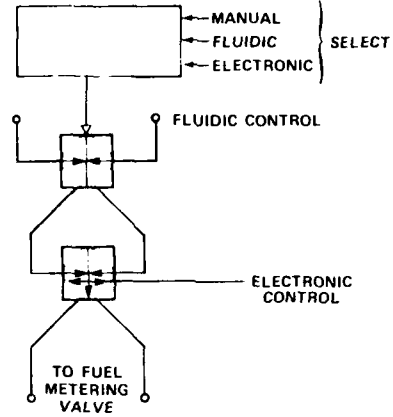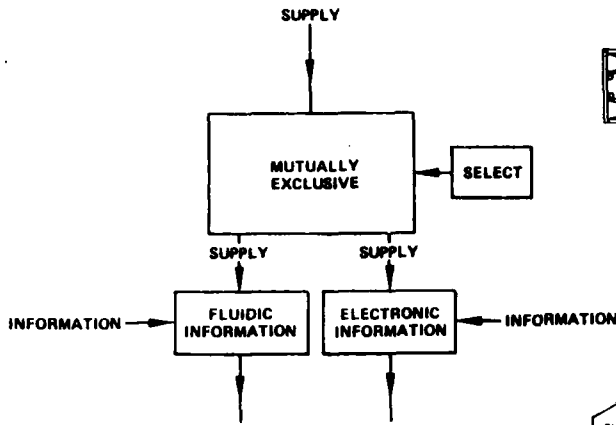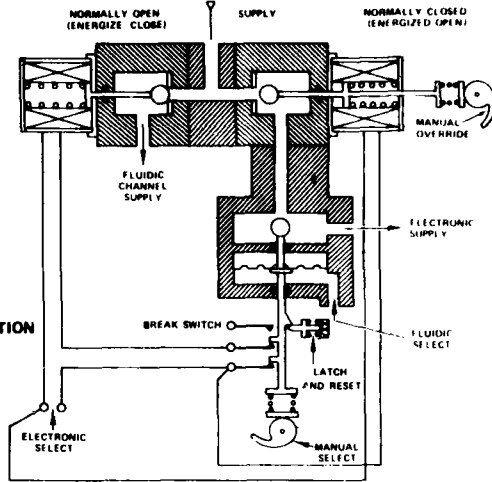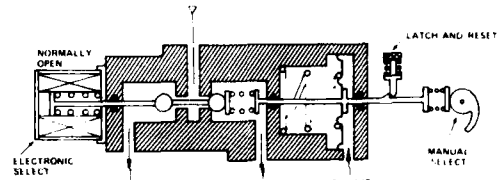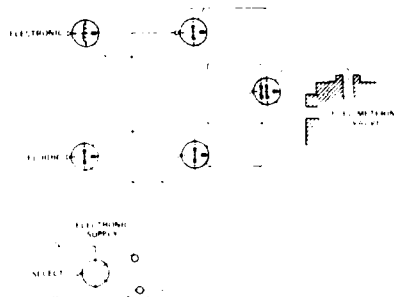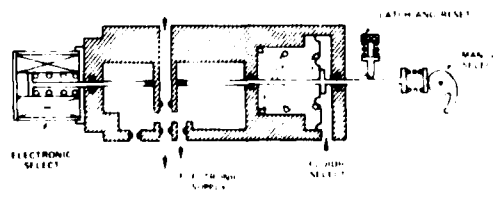### TWO SINGLE-BALL SOLENOIDS

DOUBLE-BALL SOLENOID

FLUIDIC

Figure 15.   Signal channel
supply or signal
shunt select
(Type 2).

FLEX DUCT

26

2.5.3 Type 3 Configuration

The interface of Figure 16 avoids the drawbacks mentioned in Type 1 (Figure 14) and Type 2 (Figure 15). If the fluidic channel solenoid does not seat, the fluidics may influence the electronic channel. However, if an electronic failure condition should develop, the mode selector will switch to the fluidics. There may be limitations in summing both control signals downstream.

2.5.4 Type 4 Configuration

Figure 17 illustrates a design which takes into account the drawbacks of the other designs and rectifies them.
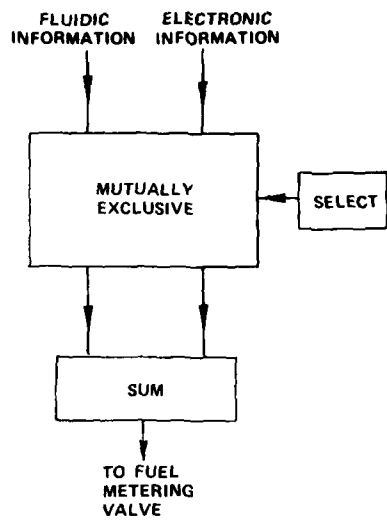
Figure 17 (Type 4) is set up in the following manner:

1. Fluidic information flows through the interface; this is to avoid any transients due to signal generation if the fluidic supply was switched.

2. The electronic channel supply is activated by the solenoid. In this manner, transients occur only during startup, and an uncalibrated E/F transducer does not influence the fluidic channel after a switch has been made.

The mutual exclusivity of channels of controls will be violated only if there is a double failure of the fluidic channel solenoid and the channel select ball and seat. A safe condition would still result since a failure condition would open the fluidic channel completely. Improper seating of the ball on the seat (if it should create a failure condition) would also result in a switch to the fluidics. The weakest point of the interface is the fluidic select diaphragm. Should it break, a fluidic switch could not be executed. The diaphragm moves only when a failure occurs; thus, the number of cycles it goes through during the operational life of the engine is very low. Therefore, the possibility of fatigue failure is low.

When power is lost or shorted out, the solenoids are de-energized. The fluidic channel is active through to the selector, and a switch can be manually executed.

27

BLOCK DIAGRAM

FLUIDIC
INFORMATION

ELECTRONIC
INFORMATION

MUTUALLY
EXCLUSIVE

SELECT

SUM

TO FUEL
METERING
VALVE

IMPLEMENTATION

HIGH-LOW IMPEDANCE SUMMING

ELECTRONIC

LOW
IMPEDANCE

FLUIDIC

HIGH
IMPEDANCE

FUEL
METER
VALVE

FLUIDIC
SELECT

ELECTRIC
SELECT

MANUAL
SELECT

FLUIDIC
CHANNEL

ELECTRONIC
CHANNEL

NORMALLY OPEN
(ENERGIZE CLOSE)

NORMALLY CLOSED
(ENERGIZE OPEN)

MANUAL
OVERRIDE

FLUIDIC SELECT

LATCH AND
RESET

FUEL METERING
VALVE

SWITCH

ELECTRONIC
SELECT

MANUAL SELECT
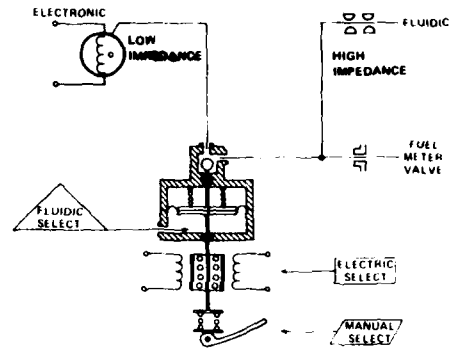
Figure 16.   Signal channel supply or signal shunt select
(Type 3).

28

BLOCK DIAGRAM

FLUIDIC
INFORMATION

ELECTRONIC
CONTROL
SUPPLY

MUTUALLY
EXCLUSIVE

SELECT

ELECTRONIC
CONTROL

ELECTRONIC
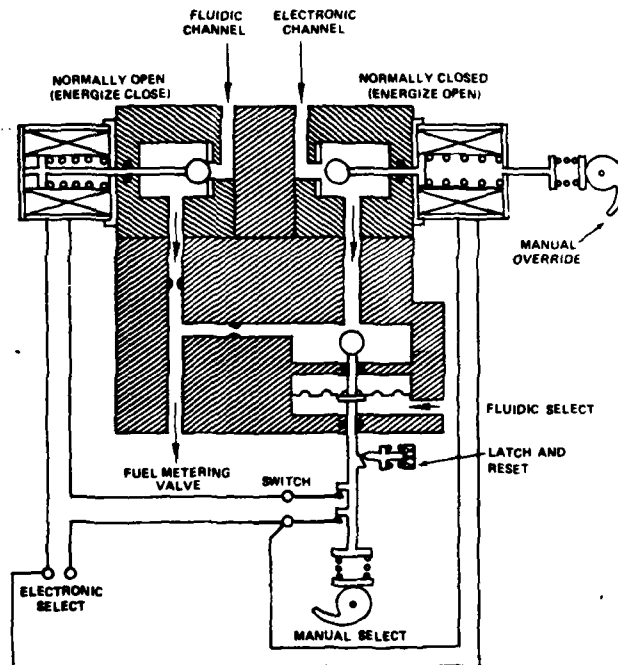INFORMATION

FLUIDIC
INFORMATION

IMPLEMENTATION
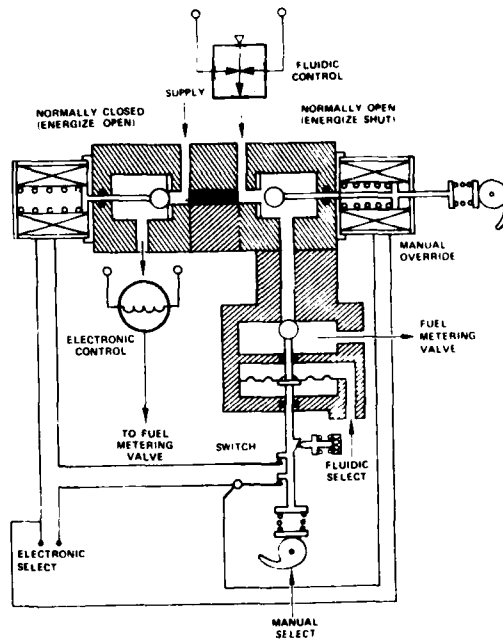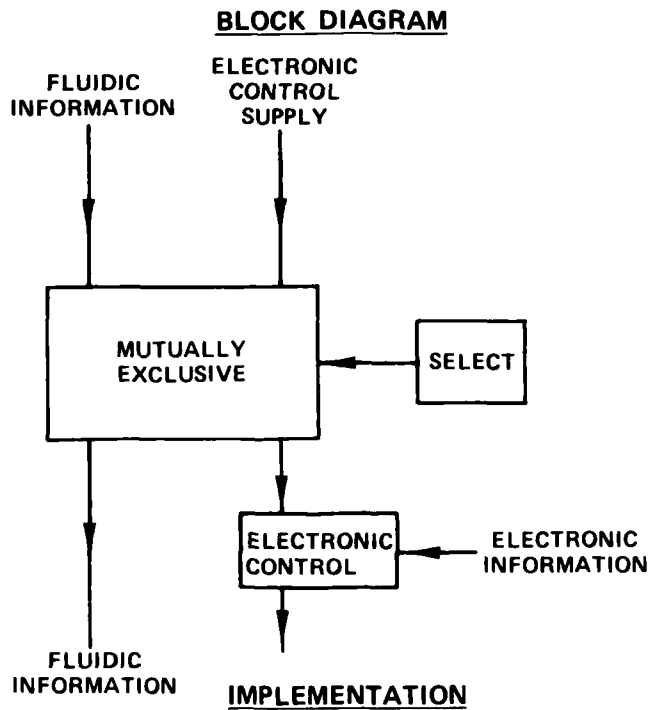
Figure 17. Signal channel supply or signal
shunt select (Type 4).

29

The electronics and fluidics will control both the fuel metering valve and the variable turbine nozzle system on the engine. The electronic control channel needs only one supply on-off control, and the fluidic channel needs a signal (on-off) control with a solenoid to open the VTN control (Figure 18).
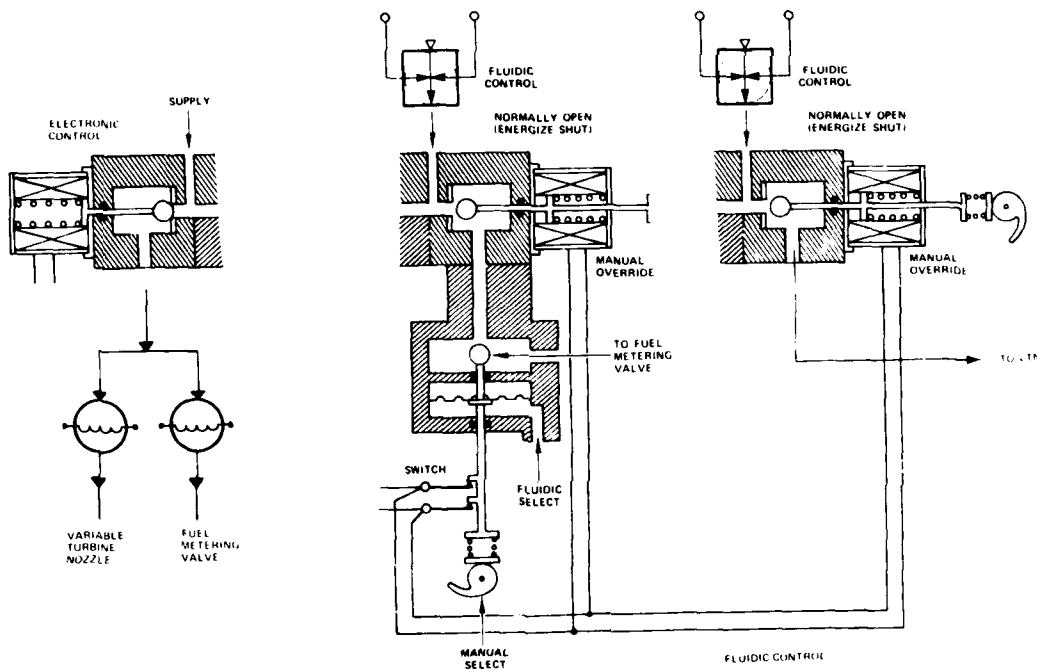
Figure 18. Electronic and fluidic control for the fuel metering valve and VTN.

The fluidic selection input would be a multiple input gate (OR gate) that would receive switch signals from the overspeed and overtemperature circuits. If the input signals are not above the switch level, the fluidic select signal would be close to zero or at a level below the minimum diaphragm force level for displacement of the ball.

30

3. LABORATORY TESTING

3.1 Pseudo-Temperature Generator

The T_4 temperature sensor is an integral part of the overtemperature signal path through which failures are detected. It is a fluidic device and is composed of a bistable amplifier with its inputs connected by a tube. When hot gas from the combustor flows across the coiled tube, the frequency of oscillation of the amplifier changes proportionally with temperature. The frequency of oscillation is related to amplifier supply pressure, the length of the tube, and temperature (see Figure 19). Because the sensed
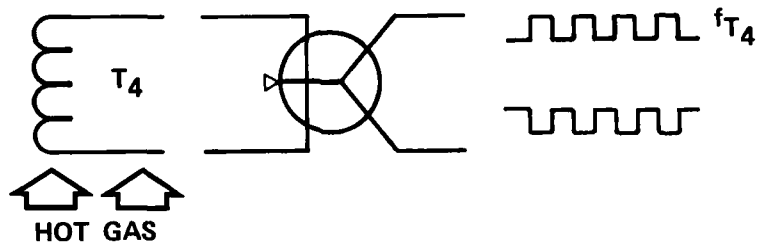
Figure 19. T_4 sensor concept.

parameter of the T_4 sensor is temperature, it would be very difficult in the laboratory to generate well-defined frequency output signals with the present sensor. The sensor would have to be placed in a combustor tube. With large thermal inertias and the difficulty of relating temperature to fuel flow, accurate calibration for testing other circuits and the entire temperature path would be very difficult to obtain.

The pseudo-temperature generator is a facsimile that enables well-defined electronic commands to be converted into T_4 circuit outputs (Figure 20). The generator works on
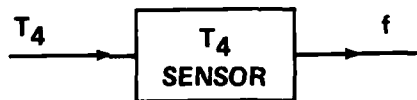
Figure 20. T_4 sensor block diagram.

31

the principle that frequency changes can be induced by changing the input connection tube length. The pseudo-temperature generator is shown in the block diagram of Figure 21.

ρ = POSITION OF TROMBONE
θ = ANGULAR DISPLACEMENT OF MOTOR
$\dot{\theta}$ = ANGULAR VELOCITY OF MOTOR
X = DISPLACEMENT OF BALL SCREW
ℓ = DISPLACEMENT OF TROMBONE
f = FREQUENCY OF T_4 CIRCUIT
LVDT = LINEAR VOLTAGE DISPLACEMENT TRANSDUCER
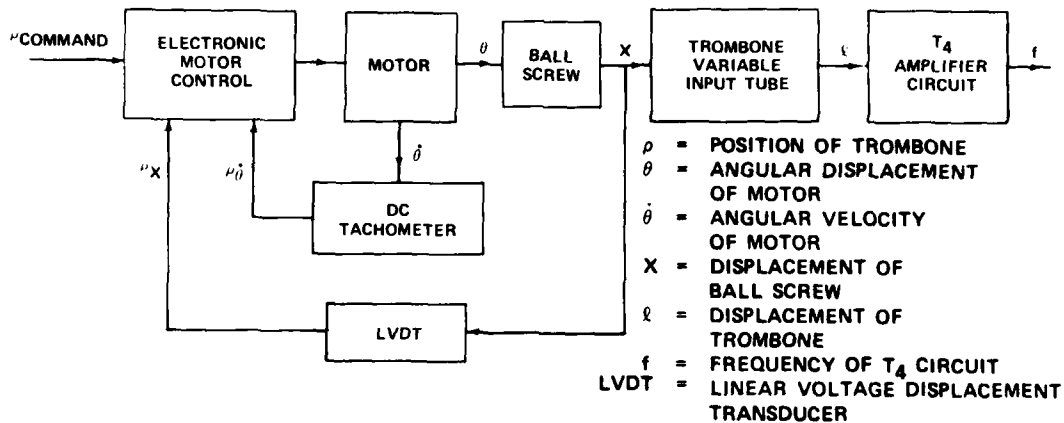
Figure 21.   Psuedo-temperature generator block diagram.

In obtaining dynamic information of the fluidic components, the trombone (variable length input tube) actuator is calibrated for maximum response within the bounds of stability.

The actual T_4 sensor has a lag related to the heat transfer characteristics of the input tubes. By adjusting the position feedback signal of the electronic controller such that there is minus 45-degree phase at the frequency of the lag, the setup can be used as a simulator. The setup shown in Figure 22 is now dynamically equivalent to the actual T_4 sensor.

Figure 22. Pseudo-temperature generator test setup.

MP-78107

3.2 Temperature Signal Path Testing

Overtemperature conditions in either T_4 or T_6 must be detected and rectified by a switch of control channels. The components comprising a temperature signal path are shown in the diagram of Figure 23.

```
OTHER SWITCHING SIGNALS
                    ┌ ─ ─ ─ ─ ─ ─ SIMILARLY T₆ FROM RECUPERATOR INLET
                    │
ELECTRICAL  ┌───────────┐  c  ┌──────────┐ wf ┌──────────┐  T₄  ┌──────────┐  NGG
──────────► │ INTERFACE │────►│   FUEL   │───►│ COMBUSTOR│─────►│   GAS    │─────►
            │           │     │ METERING │    │          │      │GENERATOR │
FLUIDIC     └───────────┘     │  VALVE   │    └──────────┘      └──────────┘
                              └──────────┘
        ┌──────────┐   ┌──────────────┐  Po  ┌─────┐  f  ┌──────────┐
        │   GAIN   │◄──│ COMPENSATION │◄─────│ F/A │◄────│    T₄    │
        │  BLOCK   │   │              │      │     │     │  SENSOR  │
        └──────────┘   └──────────────┘      └─────┘     └──────────┘
```
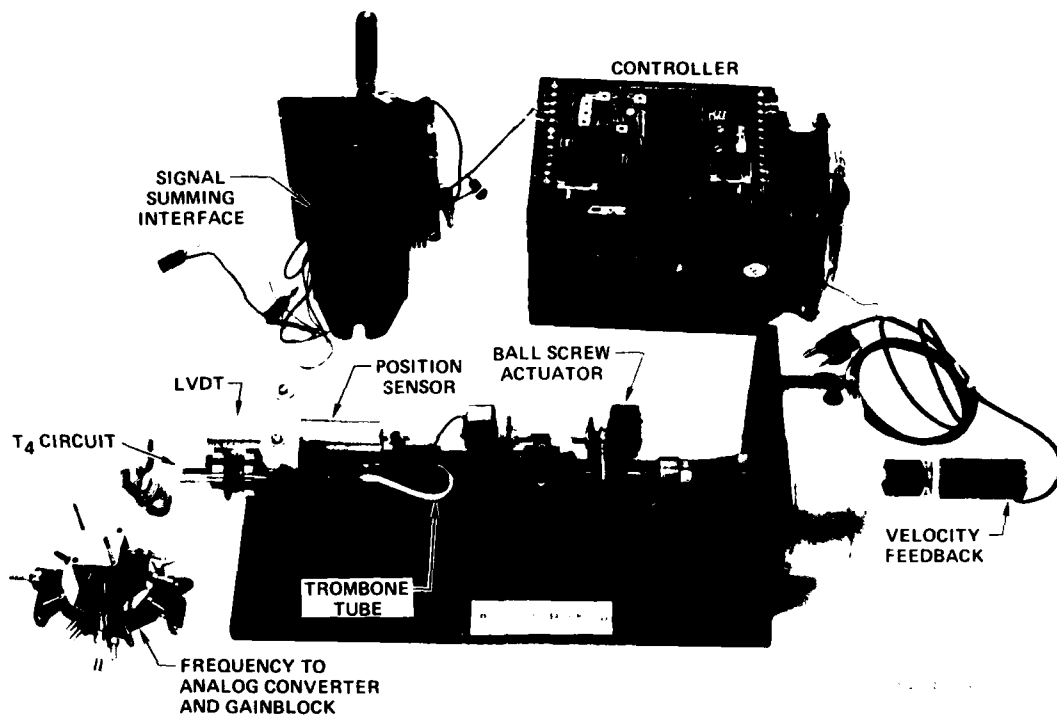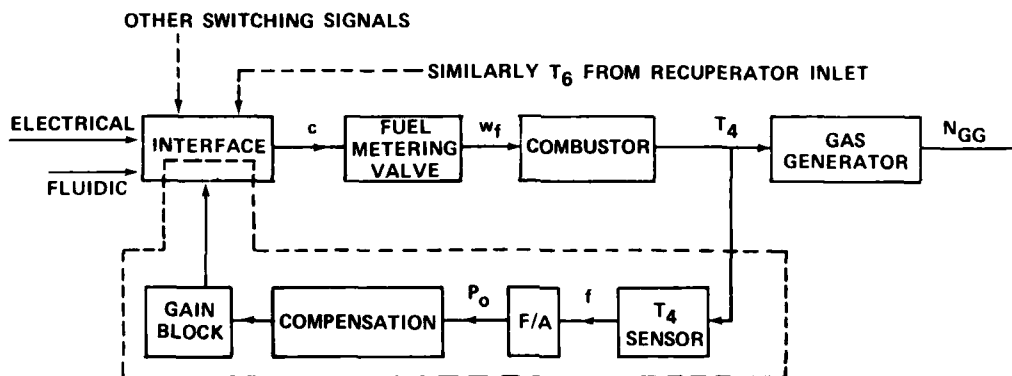
Figure 23. Temperature signal path.

Sensing T_4 overtemperature is the most critical of all the possible signals to switch on. The margin between the occurrence of a combustor event and the response of the T_4 sensor is the smallest of all the engine components and their related sensors.

The analysis showed that an overtemperature condition can be caught with a T_4 sensor with a time constant of 2.5 seconds and a compensator with a LEAD-LAG ratio of 3. When exposed to the maximum control temperature, the time constant of the actual T_4 sensor is between 0.7 and 0.8 second, indicating that a lead is not necessary and that the T_4 sensor used with a frequency-to-analog converter and gain block may be dynamically adequate.

In testing, the pseudo-temperature generator is connected to a frequency-to-analog converter and gain block (see Figure 24). Figure 25 presents a test flow graph which shows the sequence of testing.
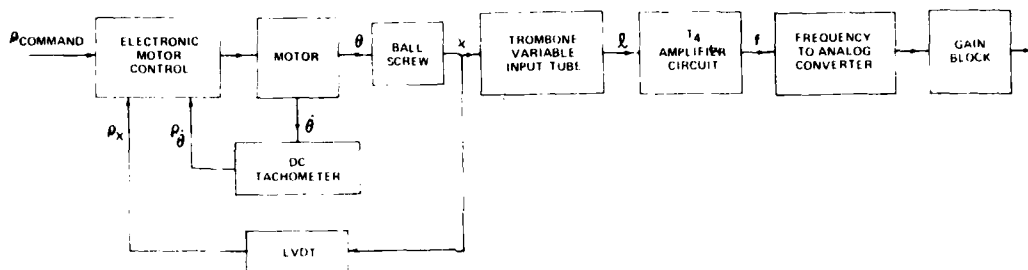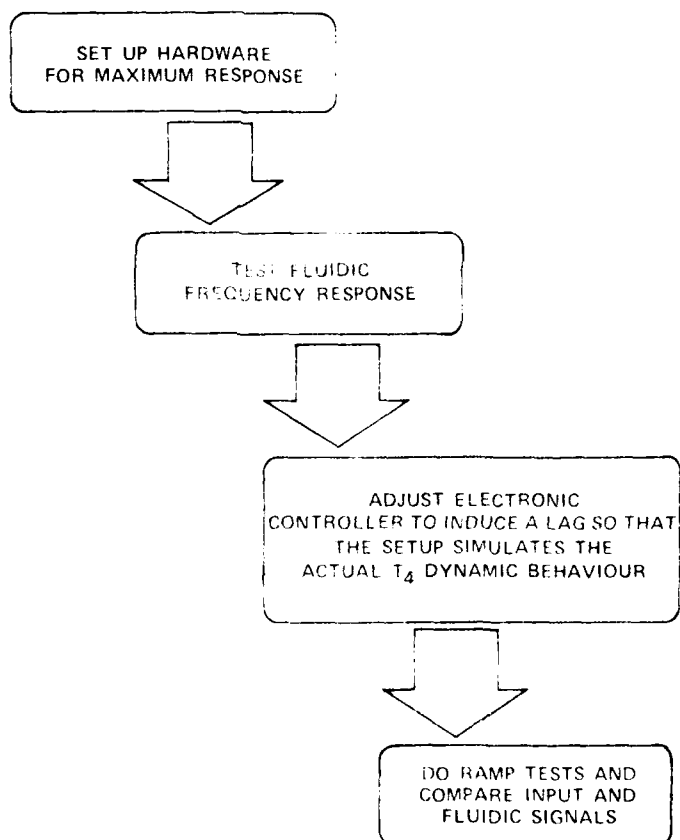
34

Figure 24. Temperature test setup.

Figure 25. Testing flow graph.

35

3.3 Temperature Sensor Test Results

The fluidic components, inclusive of the fluidics in the T_4 sensor, have the capability of responding to any signal up to 5 Hz as seen in the amplitude and phase plots (refer to Figure 26). The 0.2-Hz frequency corresponds to
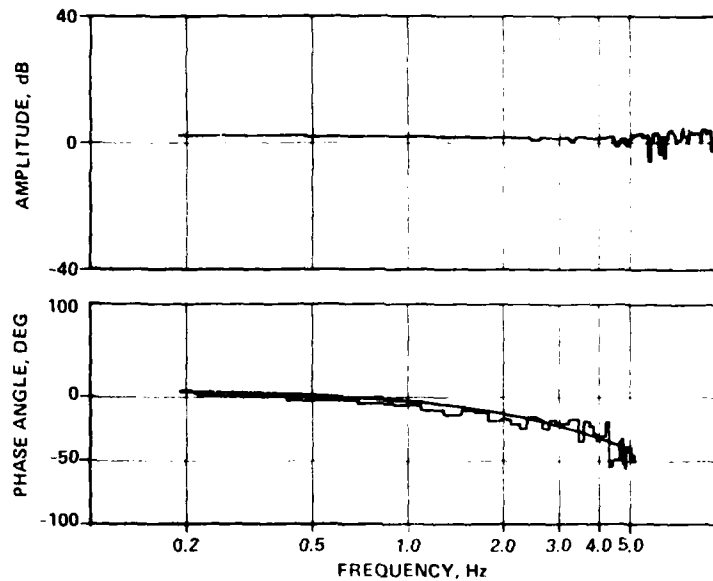
Figure 26. Fluidic components response.

the T_4 thermal lag at 1800F. From the Bode plot and the fact that normal engine cycle frequencies are well under 2 Hz, it is apparent that the thermal heat transfer lag is the most dominant concern. The fluidic components have more than adequate responsiveness.

3.3.1 Simulation Tests

The controller of the pseudo-temperature generator was adjusted so that the lag was identical to that of the actual T_4 sensor. The response sweep is shown in Figure 27.

Ramp commands were simulated by inputting a sawtooth wave. Comparisons between the fluidic output and the command were then photographed and compared on an oscilloscope.

36
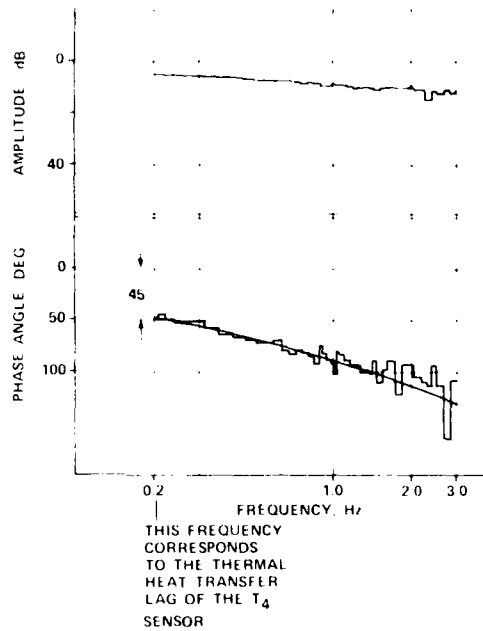
Figure 27. Response of setup and fluidics with
electronically induced lag.

The oscilloscope photograph in Figure 28 shows a 400-degree-per-second rate of change of temperature. The fluidic signal is following the simulated temperature in the manner of simple delay 0.07 to 0.10 second behind. The amplitude of the noise is about one-fifth that of the 20F signal band of noise.
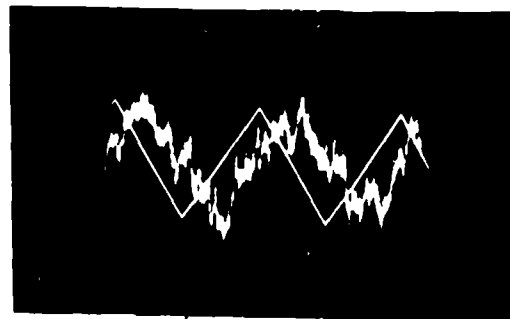
RAMP IS 0.25 S LONG.
TOTAL CHANGE OF OUTPUT
IS 20 Hz (120F).

0.5 S

Figure 28. Temperature ramp simulation.

37

The maximum control temperature for T_4 is between 1800F and 1880F, depending on ambient conditions. The highest control temperature occurs at altitude on a hot day. The engine can withstand temperatures of near 2100F, but only for periods of less than 20 seconds. Using the delay time of 0.07 to 0.10 second and a noise band of 20F as seen in Figure 27, an appropriate switch point or necessary level can be determined.

During normal operating conditions, the gas turbine engine generally sees T_4 temperature rates of less than 200 degrees per second. Figure 29 shows a rate envelope between 200 and 1000 degrees per second.
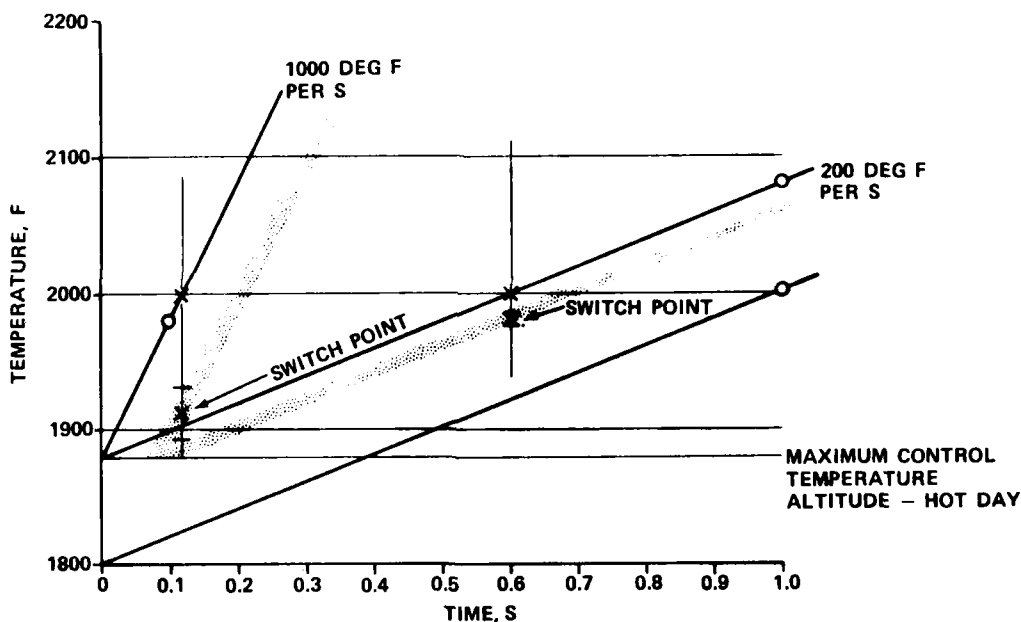
Figure 29. Overtemperature switching margins.

To avoid a T_4 temperature level of 2000F when the temperature is increasing at a rate of 1000 degrees per second, the switch point must be set between 1895F to 1930F and, for a 200 degrees per second rate, the switch point must be set no higher than 1990F (see Figures 30 and 31). Possible switch points would fall between the 1980F to 1895F levels
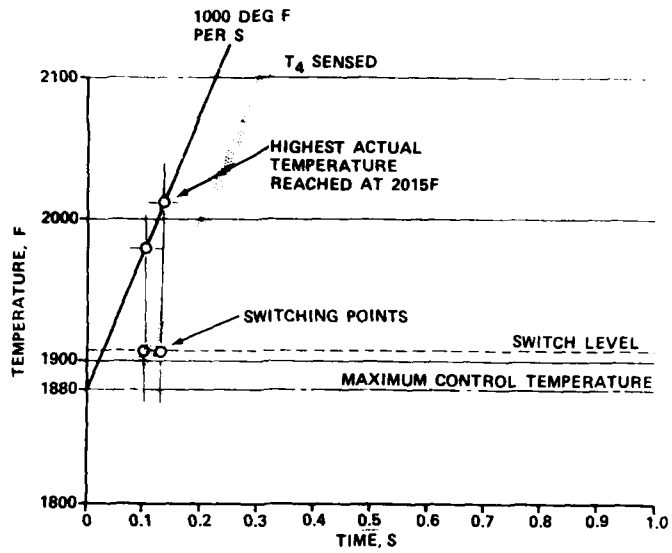
Figure 30.   High rate switch point.
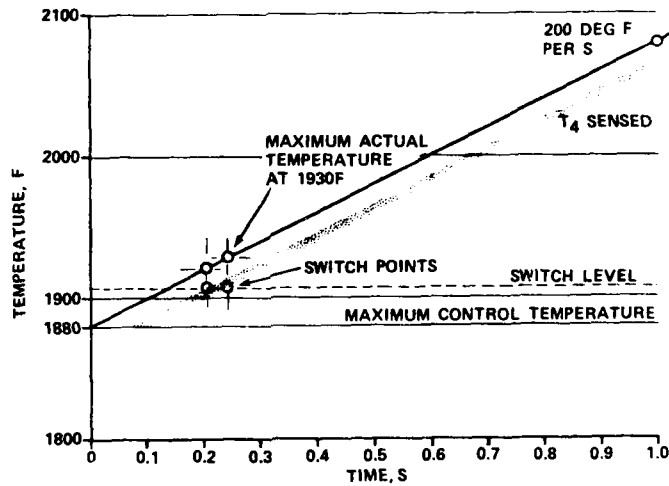
Figure 31.   Low rate switch point.

39

of the control temperature envelope. Allowing for noise and some margin, a switch point of 1900F to 1910F can accommodate temperature rates up to 900 degrees per second beyond which there would be some overshoot (see Figure 32).
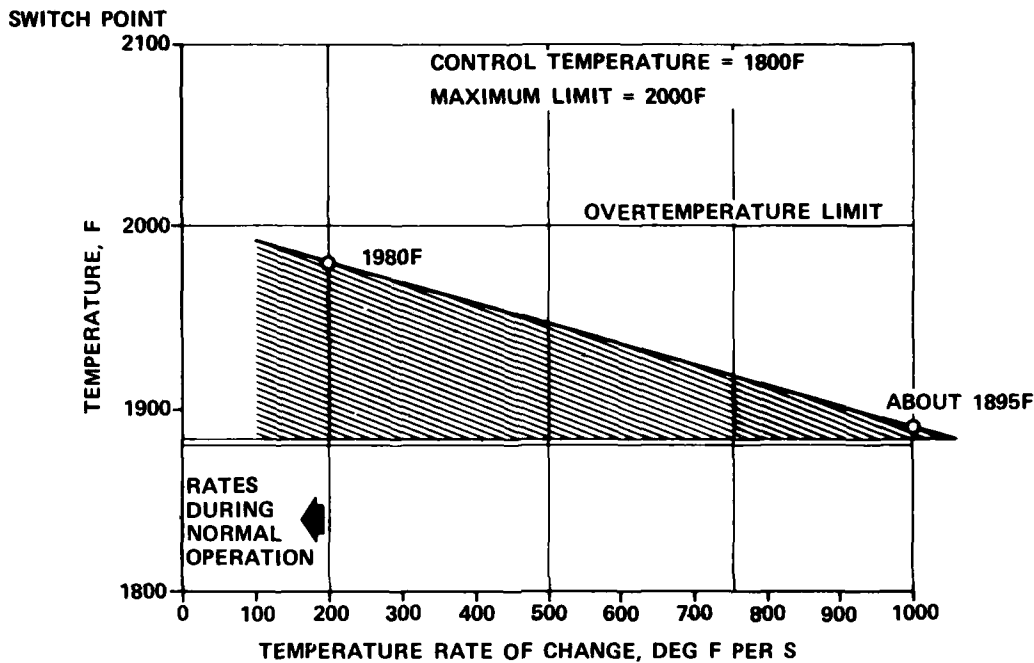
SWITCH POINT

Figure 32. Switch points for different temperature rates of change.

A switchpoint should be chosen such that it is beyond normal noise excursions and yet as close to the normal control temperature as possible to minimize the maximum actual temperature overshoot.

From Figures 30 and 31, it can be seen that, by choosing a 1910F switchpoint, temperature overshoots from the maximum control temperature (at rates near 200 degrees per second and slower) can easily be rectified. The maximum actual temperature should not exceed 1930F. Should temperature rates five times those normally seen in engine operation occur, the maximum overshoot temperature would be limited to 2015F.

40

3.4 Speed Sensor

The laminar amplifier/disc speed sensor is investigated here as a means of obtaining accurate speed information. Because of the simplicity of design, separate speed channels for control and speed limiting are possible; therefore, packaging and adaptation of the sensor to an engine is relatively easy. Any exposed shaft may be used for a speed pickoff, and the number of pickoffs per shaft is limited only by the relative size differences between the sensor amplifiers and the number of amplifiers that can be clustered around or placed axially along the shaft.

The sensor amplifier stack may be clustered around an open shaft as in Figure 33 or sealed in a closed package around the roller or disc as shown in Figure 34. In the latter case, the disc may be coupled through a magnetic drive coupling from a shaft within the engine gearbox or from a splined shaft at an accessory mount pad.
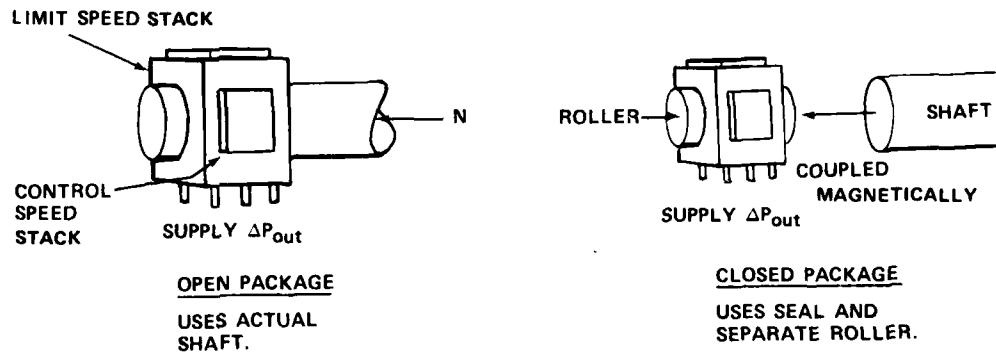
Figure 33.   Open package speed sensor.

Figure 34.   Closed package speed sensor.

3.4.1 System Description

The boundary layer flow generated by a one-inch-diameter disc was found to be sufficient to drive a typical laminar amplifier. Flow generation of various surfaces is shown in Figure 35. A cylindrical roller (disc) was used in this study due to its similarity to a shaft. The boundary layer flow from the disc is used as a crossflow over the interaction region of the amplifier shown in Figure 36. The crossflow deflects the power jet flow and creates a differential output pressure that is proportional to shaft speed.

41
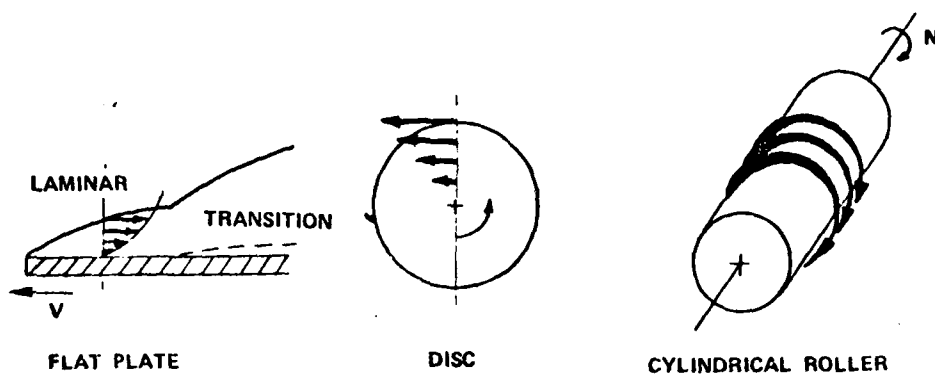
Figure 35.   Classes of moving surfaces for a laminar
amplifier/disc speed sensor.
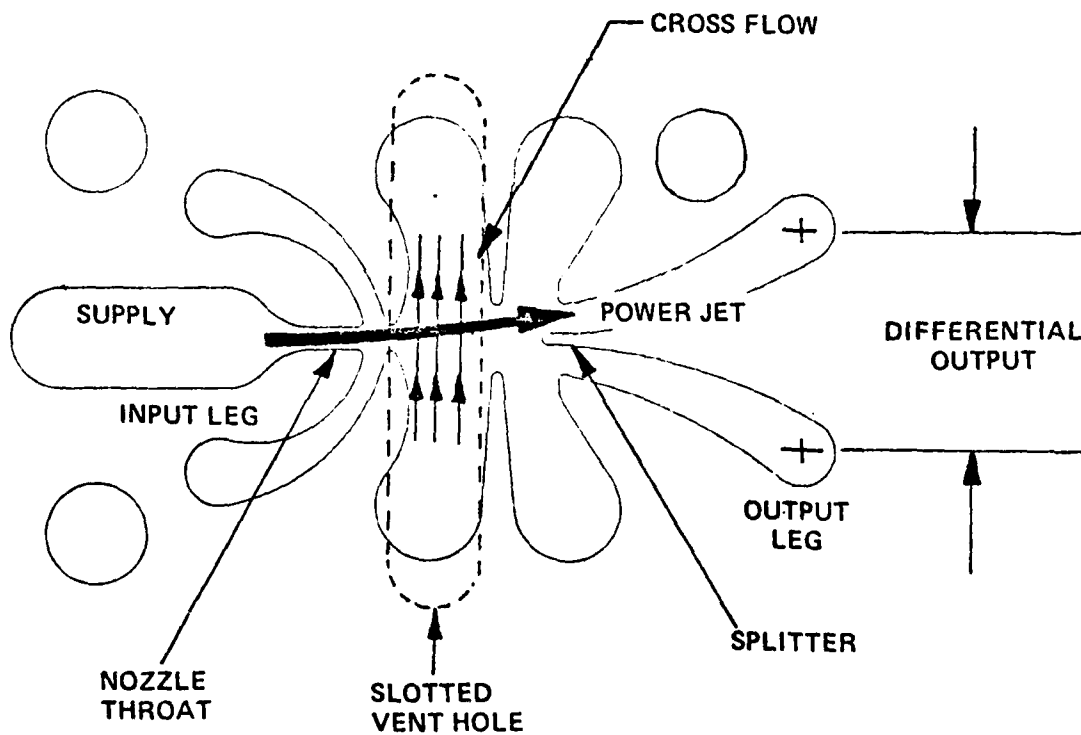
Figure 36.   Interaction region of fluidic amplifier.

The sensor's two major parts are a disc and a laminar
amplifier which are shown in Figure 37. The disc sits above
a brazed amplifier assembly and influences the amplifier
through the open vent slot. The effects of axial offset in
alignment and axial rotation can be seen in Figure 38.
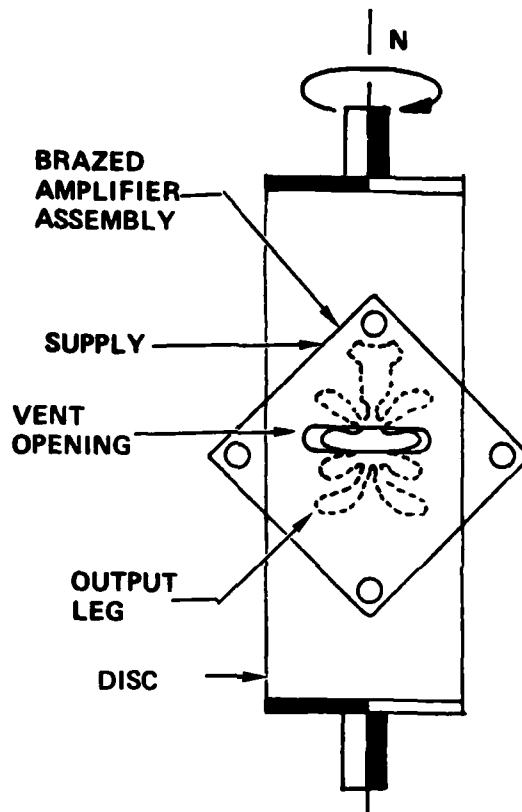
Figure 37.   Disc and laminar amplifier.

Moving the disc, rotating counterclockwise, to the
right of the centerline of the axis of rotation increases
the nonlinearity of the speed-pressure relationship and
moves the curve to the right. Moving the roller to the left
by an equal amount increases the nonlinearity in the
opposite direction. Movement away from the centerline in
either direction increases the noise level in the upper
limits of the speed range and reduces the range of a useful
signal. Rotating the axis of rotation of the disc in either
direction away from the centerline of the gap has a similar
deteriorating effect on performance.

43
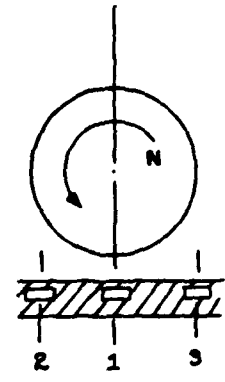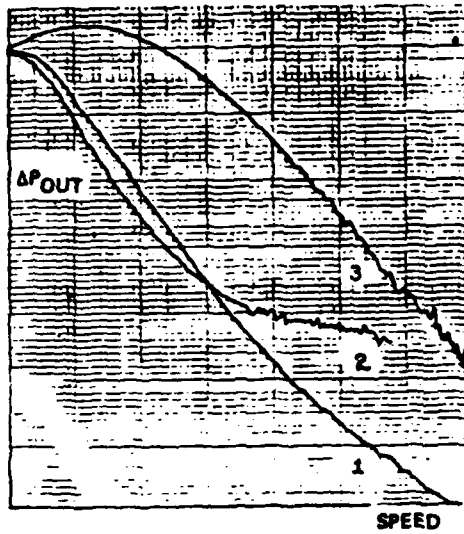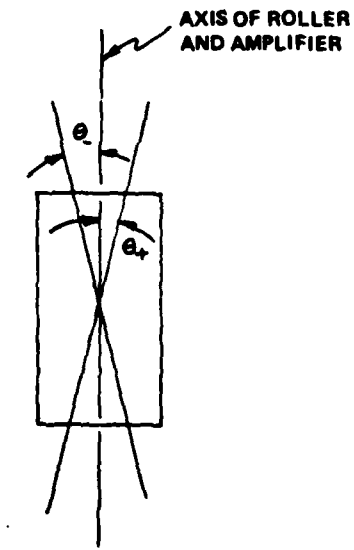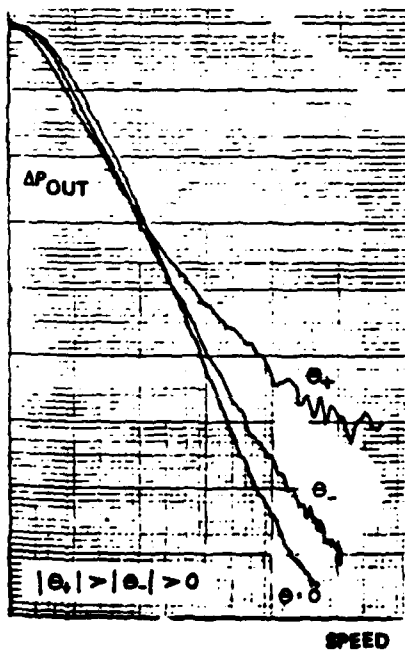
Figure 38.   Effects of axial offset and axial
              rotation.

44

3.4.1.1 <u>Critical Parameters</u> - For a given amplifier power jet nozzle area, there is an optimal gap and maximum roller diameter. The gap is the distance from the disc surface to the top of the amplifier nozzle shown in Figure 39.
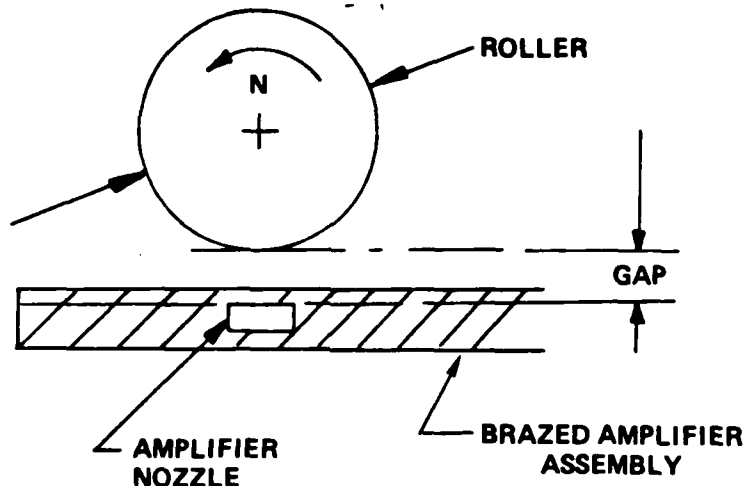
Figure 39. Gap distance for laminar amplifier/disc speed sensor.

The optimal gap depends on the velocity profile which develops around the disc. If the gap is too large, there may not be sufficient momentum exchange to drive the amplifier through its full range.

The maximum disc diameter relates to velocity profile development and the need to keep the crossflow from going into turbulent transition, thus generating noise.

The sensor's sensitivity at a given supply pressure and aspect ratio (flow area) decreases with increasing gap (see Figure 40). The sensor's optimal gap is a tradeoff between the highest sensitivity obtainable (as small a gap as possible) and the noise or output variations due to disc runout.

In applications where the need for high shaft-speed-to-amplifier output gain (which increases with disc diameter) requires a large disc diameter, a boundary layer inhibitor
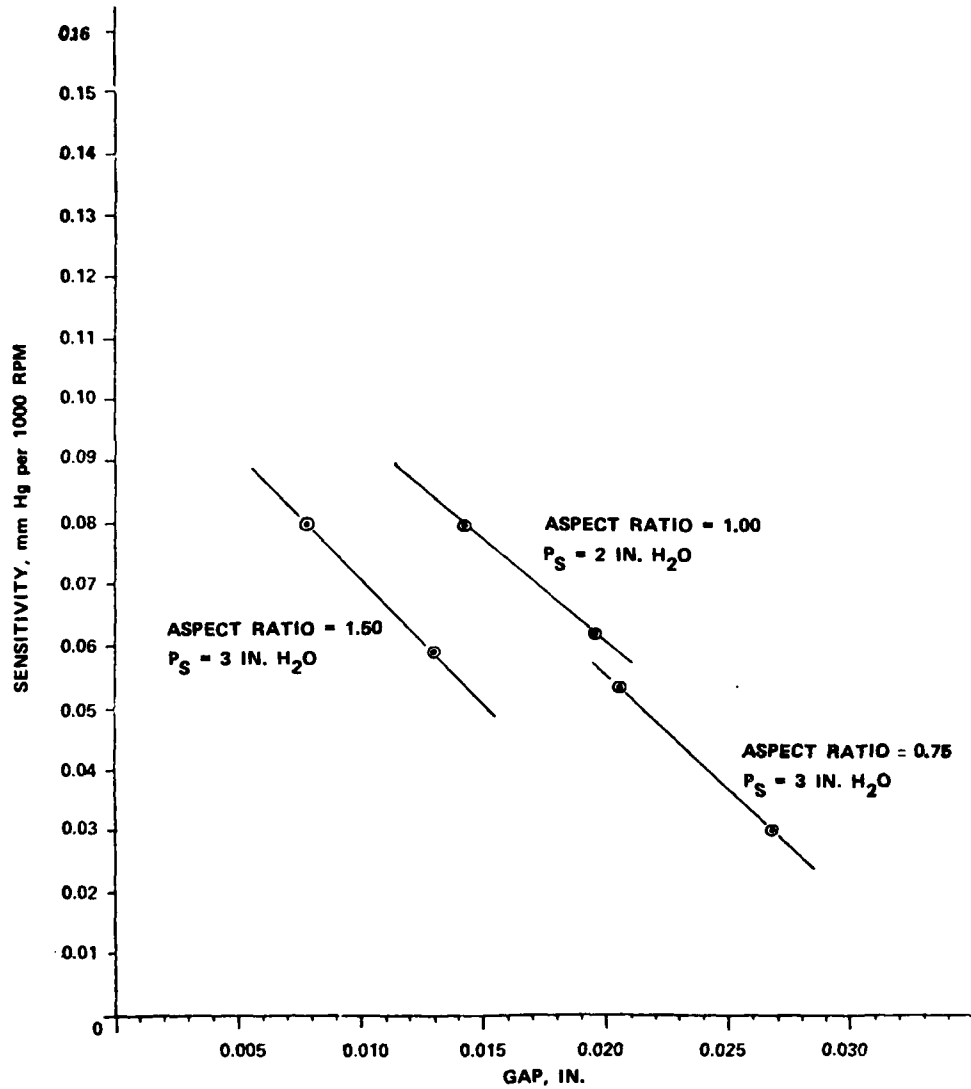
Figure 40. Sensitivity versus gap.

can be used as shown in Figure 41. The inhibitor can either completely suppress the velocity profile generated by the roller, or suppress it sufficiently to prevent transition.

46
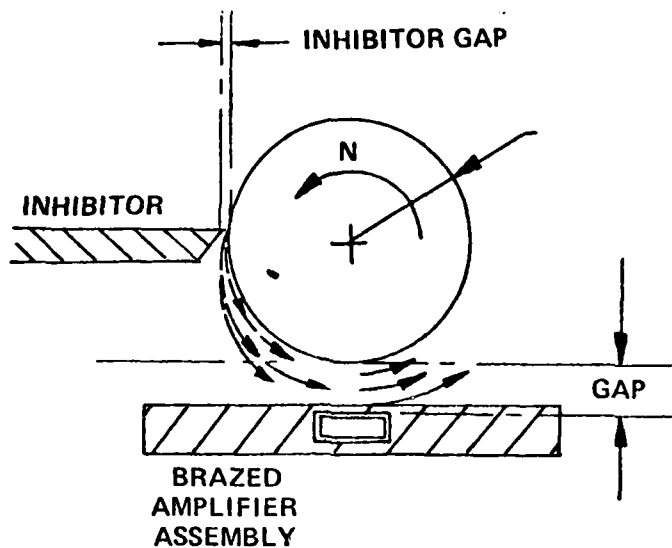
Figure 41. Boundary layer inhibitor.

Figure 42 shows the output signals of the sensor at various inhibitor gaps. Placement of the inhibitor is critical only in preventing transition. Placing it closer to the inter-action point slightly decreases gain.

3.4.2 Vent Geometry

Five types of vent geometries were evaluated: small circle, large circle, open square, slot, and vent contour (see Figure 43).

The power jet is influenced more when the opening is closer to the power jet nozzle. A fluid particle has more time to move laterally in the flow direction when it is farther away from the splitter.

Noise increased proportionally with increased exposure of the vent region. The slotted vent had comparatively good operation and less noise development. The slotted vent best accommodated the crossflow by eliminating velocity com-ponents except for those directed perpendicularly toward the power jet.

47
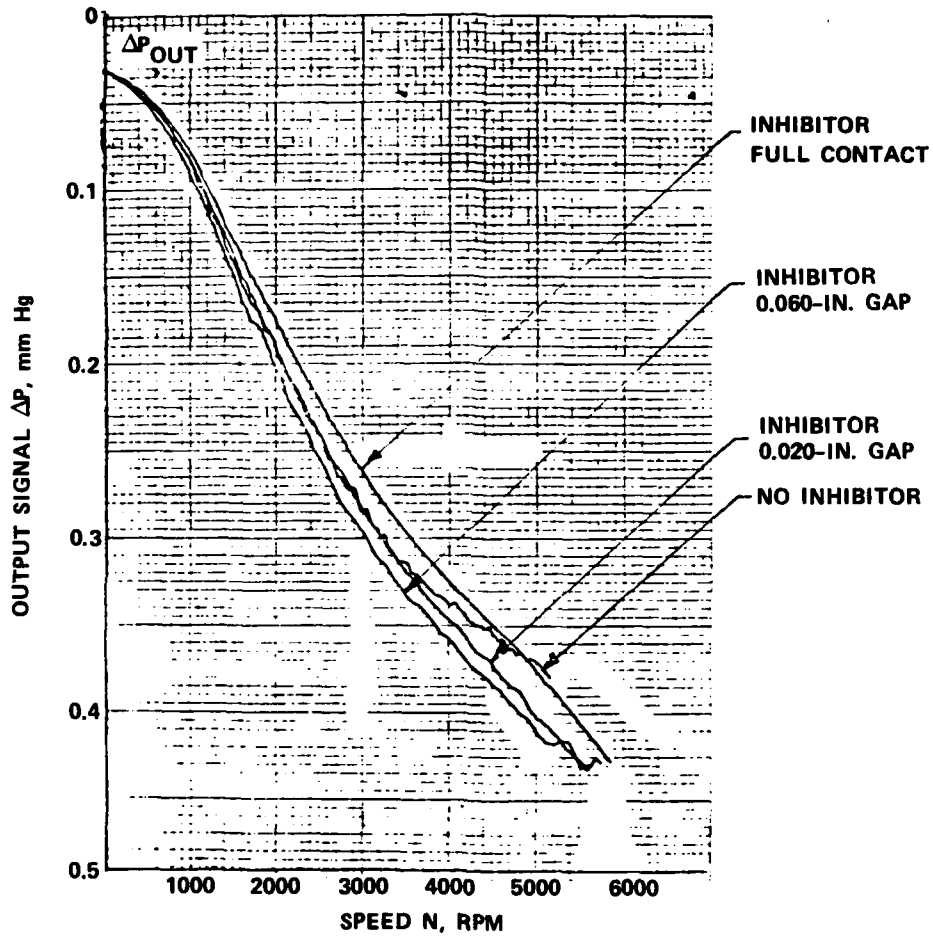
Figure 42.   Effects of inhibitor.
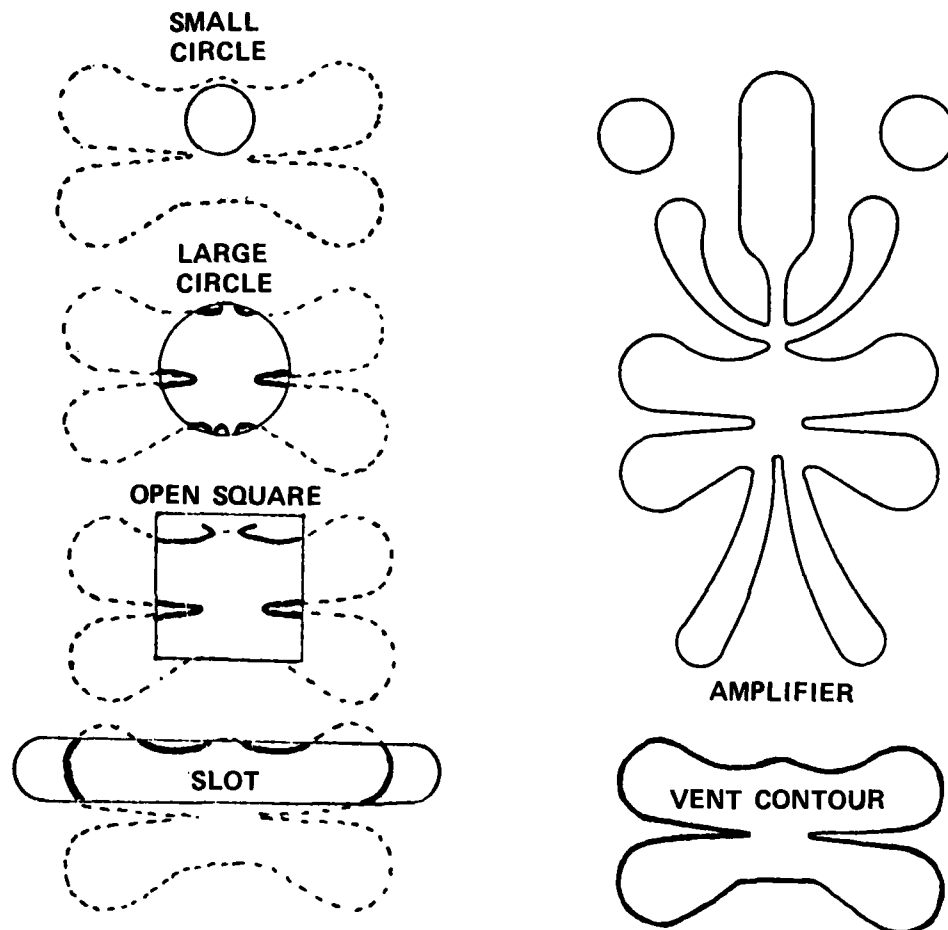
Figure 43. Vent geometries for a fluidic amplifier.

3.4.3 Aspect Ratio

The best usable linear range of operation and the max-
imum linear output occurred when using an amplifier assembly
with a throat aspect ratio of one (see Figure 44). Outputs
of amplifiers with smaller or larger aspect ratios were less
linear.

49
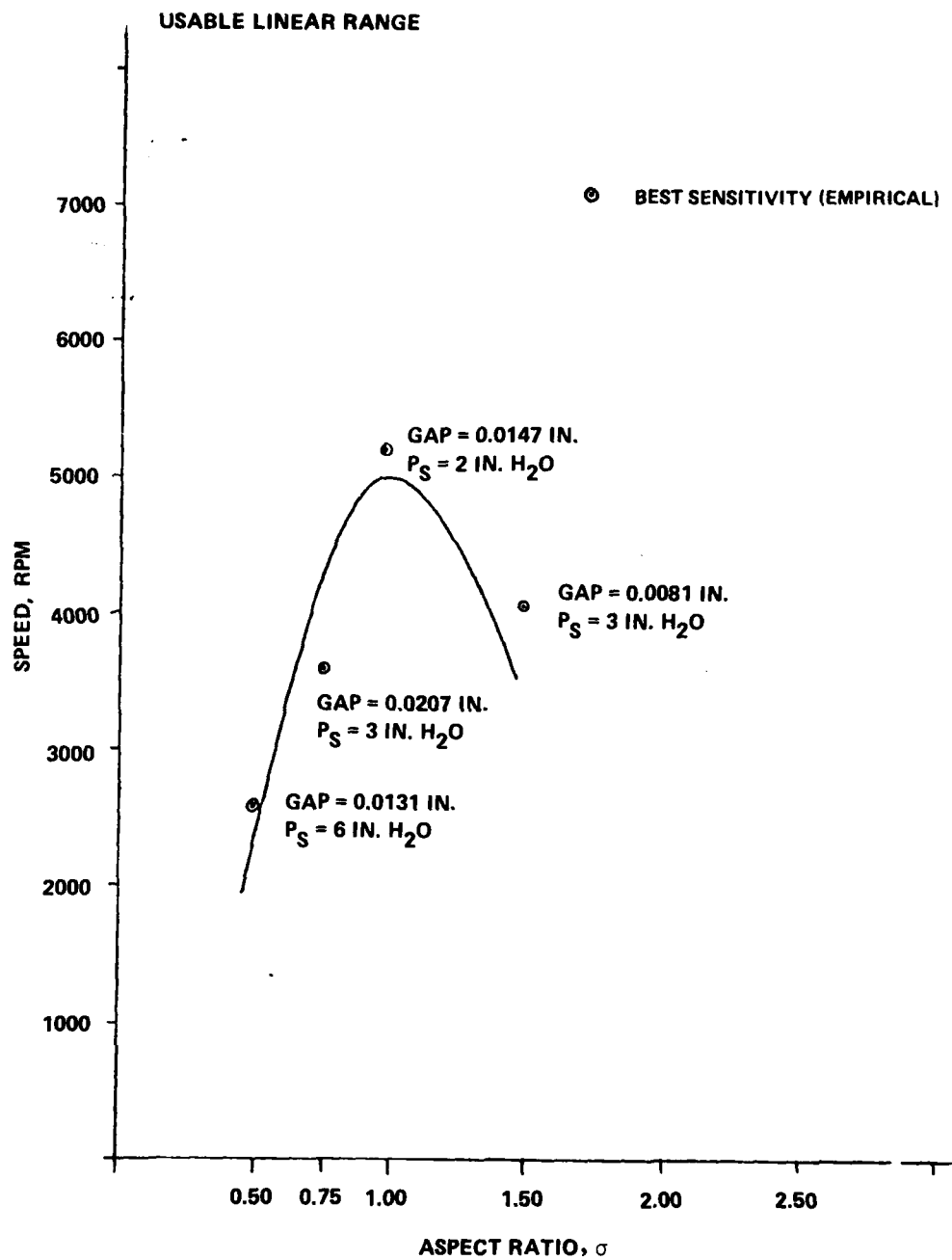
Figure 44.   Linear range versus aspect ratio.

3.4.4 Test Results

A unit composed of a one-inch-diameter disc and a 0.02 x 0.02-in. power nozzle amplifier (Garrett Part 3155131) was used to test the concept. An inhibitor was placed in full contact with the roller one-quarter turn in front of the disc-vent region. The disc was aligned with no axial offset or rotation. Under these conditions with pressure supply at 1.0705 mm Hg (2.0 in. H_2O), the sensor demonstrated the performance shown in Table III.

TABLE III. LAMINAR AMPLIFIER/DISC SPEED SENSOR

Parameter	Figure 45	Typical Values
Optimal Gap	0.015	0.009 to 0.014 in.
Usable ΔP Linear Range	0.25-0.30	0.20 to 0.40 mm Hg
Sensitivity $\dfrac{mm\ Hg}{1000\ rpm}$	0.062	0.060 to 0.080
Signal-to-Noise Ratio		300:1 over 4750 rpm speed range

Curves of the best design configuration are shown in Figure 45. The noise at the low speed saturation is due to the bearing mount. The noise at the high speed saturation is due to turbulent transition.

A laminar gain block can be used to increase the gain of the low level output signal up to a usable range. The output signal-to-noise ratio is quite high and a gain block should not add significantly to the noise level. Laminar gain blocks with gains in excess of 10^6 are realizable; therefore, reaching usable levels of output is not a problem.

3.4.4.1 Speed Sensor and Temperature Sensitivity – A test rig with a closed housing for the disc was built for temperature testing the laminar speed sensor (see Figures 46 through 49). The matrices of combinations of temperature between the disc boundary air layer and the amplifier through-flow are shown in Figure 50.

51
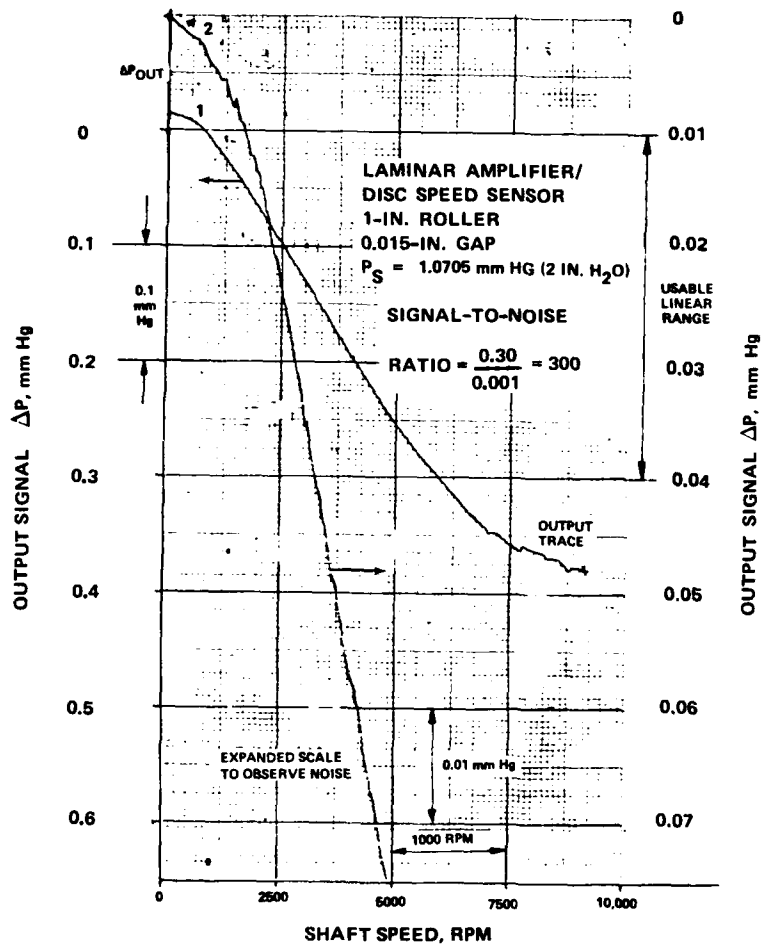
Figure 45. Performance of laminar
amplifier/disc speed
sensor.

52
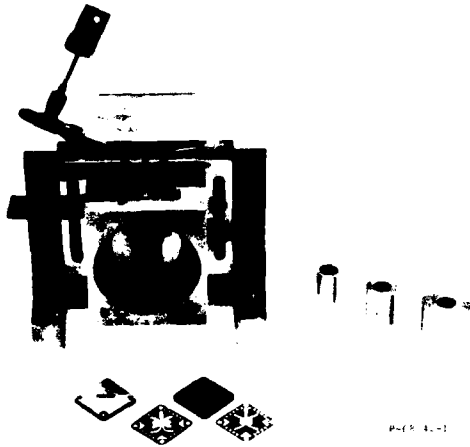
Figure 46. Roller speed sensor test setup.

Figure 48. Side view of test housing.
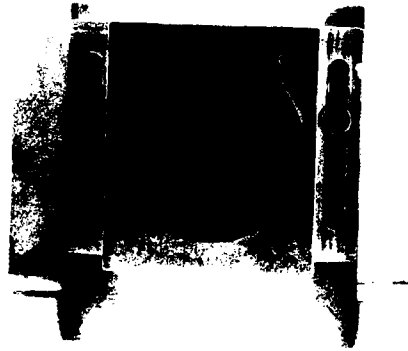
Figure 47. Front view of test housing.

Figure 49. Top view of test housing.

53
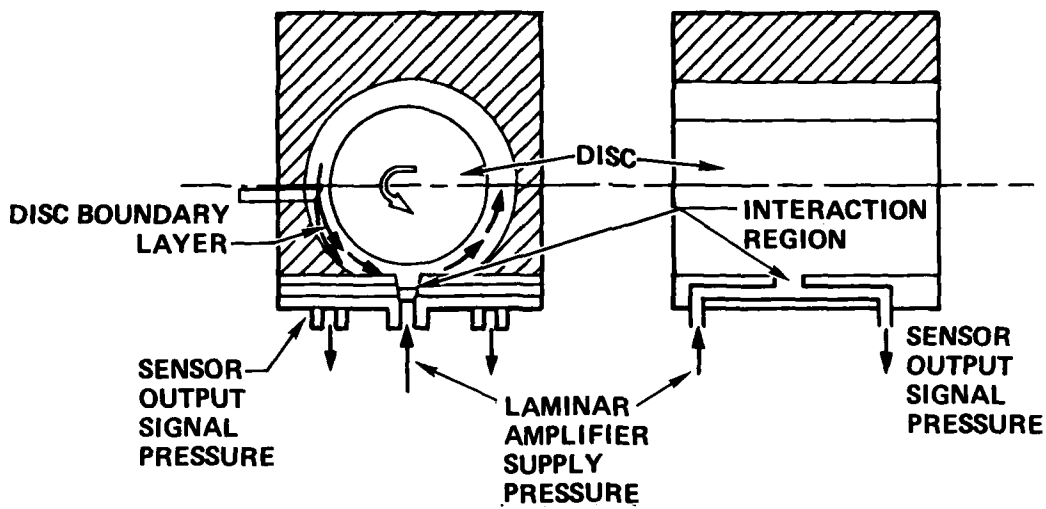
DISC BOUNDARY LAYER FLOW

	AMBIENT	HOT
HOT	FIGURE 53	FIGURES 54, 55
AMBIENT	FIGURE 45 (PROTOTYPE AMPLIFIER)	FIGURE 52

LAMINAR AMPLIFIER SUPPLY FLOW

Figure 50. Temperature testing matrix.

The heating of the amplifier air supply gives information on the effects of Reynolds number changes in the power jet. Heating the ambient air should affect the behavior of the crossflow air. The results shown in Figures 51 through 54 indicate very little change in sensitivity or signal-to-noise ratio with the output signal over the full range of temperatures tested. In the hot supply/ambient boundary layer plot, a temperature difference as high as 200F does not significantly affect the sensor.
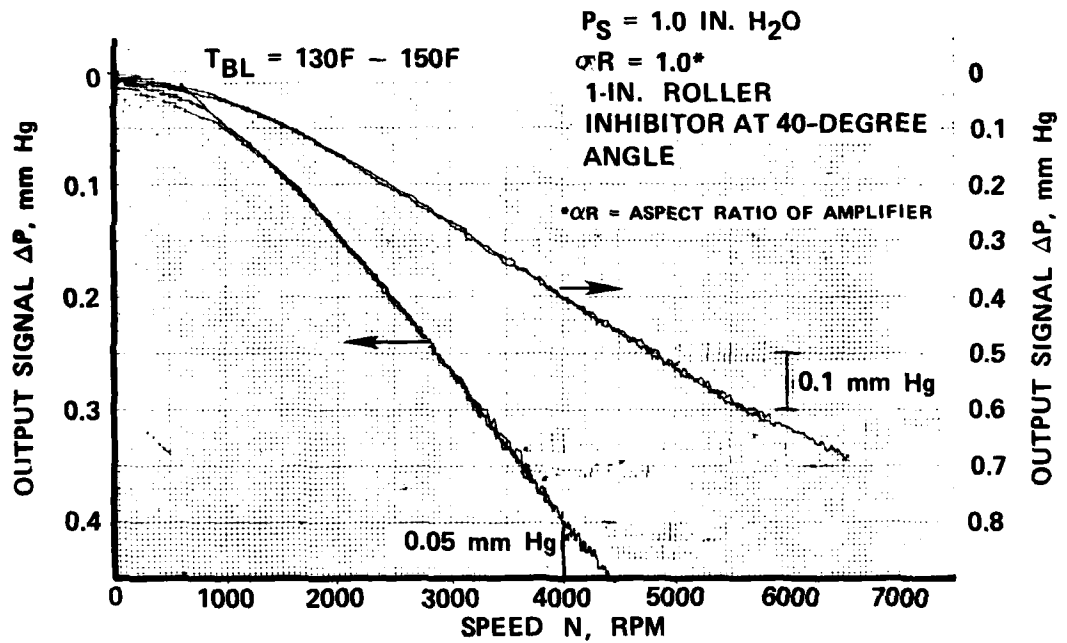
Figure 51. Sensor temperature test: hot boundary layer, ambient amplifier supply.
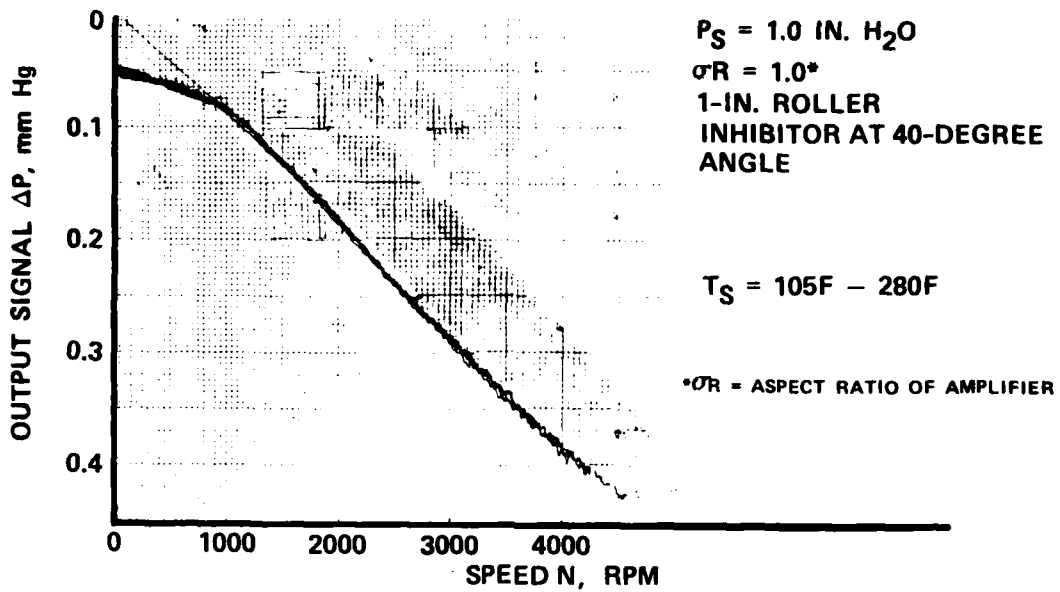
Figure 52. Sensor temperature test: ambient boundary
layer, hot amplifier supply.
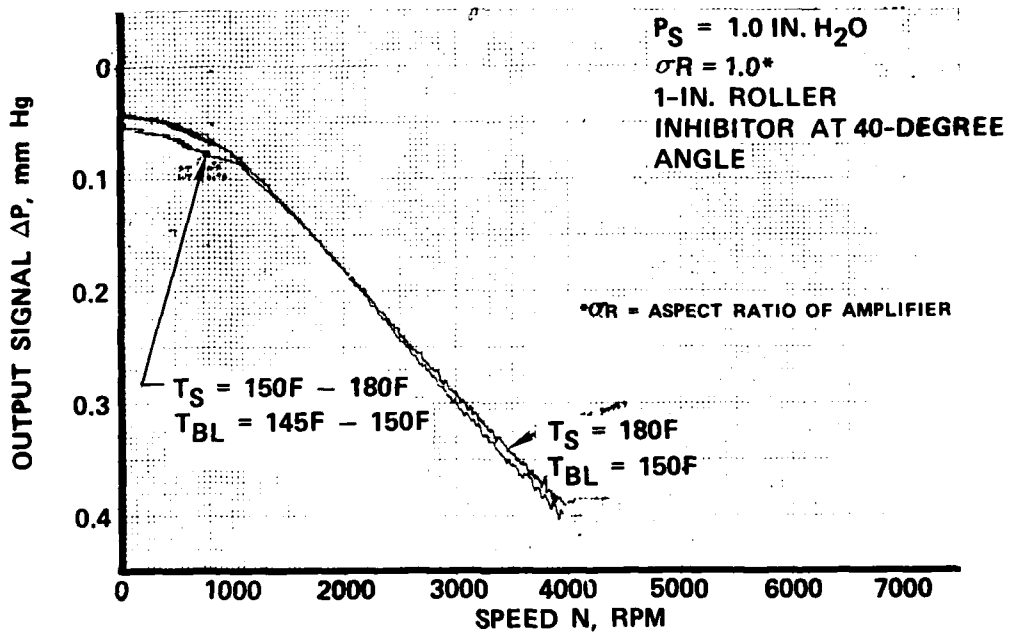
Figure 53. Sensor temperature test: hot boundary
layer, hot amplifier supply.

56
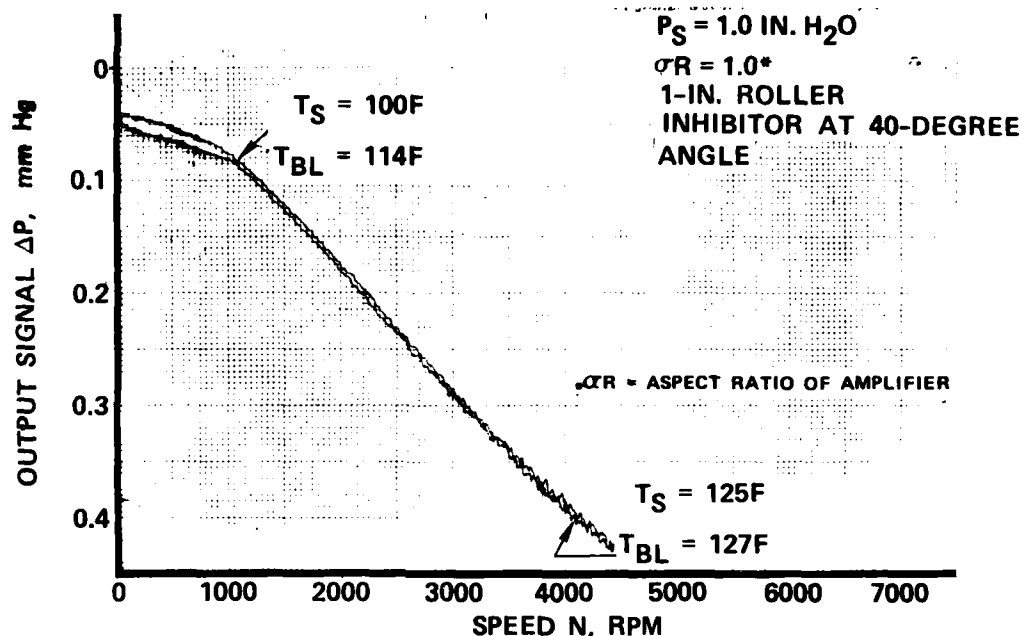
Figure 54. Sensor temperature test: hot boundary
layer, hot amplifier supply.

4. CONCLUSIONS AND RECOMMENDATIONS

The evaluation and testing conducted during this phase
of the program has shown that, with state-of-the-art
fluidics, critical gas turbine engine failure modes can be
detected and automatic switching to a fluidic control can
be accomplished. Interface of all engine control sensors
can be accomplished for fluidic fuel metering and variable
turbine nozzle control.

Speed sensing accuracy required for GT601 gas turbine
engines can be obtained using the laminar amplifier/disc
speed sensor. Its signal-to-noise ratio is high and the
output signal can be biased by controlled jet inputs, making
the sensor adaptable to speed governing. The combined per-
formance of the sensor and laminar gainblock needs to be
evaluated when metering valve operating pressures are known.
It is expected that both usable signal levels and good
signal quality can be obtained. Because of the simplicity
of its design, any number of sensor circuits can be
clustered on a single shaft to provide speed control and
limiting.

57

The overtemperature conditions that might occur in engine failures are the most demanding. Because of its heat transfer nature, the response of a temperature sensing device is inherently slow. The T_4 sensor and failure deflection circuits were found to be capable of responding to temperature rates nearly five times faster than changes seen during normal engine operation. From the standpoint of circuit improvement either electronically or fluidically, a device (the electronic or fluidic analog) as illustrated in Figure 55 should be investigated in conjunction with the T_4 failure circuits.
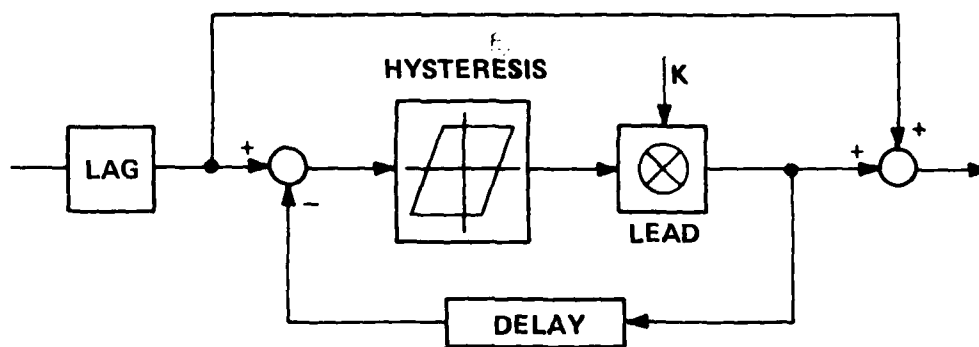
Figure 55. Lag-lead with hysteresis.

The circuit will enable the addition of lead to the temperature signal without the increase of noise level in the range of frequencies where the lead is active. In this manner, the response of the temperature sensor can be increased without a loss of signal accuracy.

The fluidic circuits used in this study were evaluated from the standpoint that failure conditions would be sensed and a critical situation avoided by switching channels of control information. It is advantageous for the long term scope of this program to examine the possibilities of other direct and localized controls for correcting failure conditions. An example is in the case of an overtemperature condition where the VTN could be directly commanded by the failure circuit to open (at least momentarily) and hence drop the temperature while the switch is being executed. This kind of approach may further increase the ability of switching channels safely in the dual-channel control approach.

ABBREVIATIONS, ACRONYMS, AND SYMBOLS

BL	boundary layer
f/a	frequency-to-analog
F/A	frequency-to-analog converter
IGV	inlet guide vanes
K_{GG}	gas generator torque-speed gain
N	speed, rpm
N_{GG}	gas generator speed
N_{PT}	power turbine speed
P_O	discharge pressure
P_S	supply pressure
Q_{GG}	gas generator torque
s	Laplace transform operator
S	switch and interface delay
T	temperature
$T_{3.5}$	combustor inlet temperature
T_4	gas generator inlet temperature gas generator turbine inlet temperature, gas generator inlet overtemperature, gas turbine inlet overtemperature, T_G inlet temperature
T_{4C}	compensated gas turbine inlet temperature
$\dot{T}_4$	gas generator inlet temperature change rates

ABBREVIATIONS, ACRONYMS, AND SYMBOLS (CONT'D)

T_6	recuperator inlet temperature
T_P	turbine temperature
VTN	variable turbine nozzle
w_f	fuel flow
σR	aspect ratio of amplifier
ΔP_{OUT}	differential output pressure
θ_+	effects of axial rotation
θ_-	axis of roller and amplifier
τ	time constant
τ_C	combustor fuel residence time
τ_{CH}	chopper time constant
τ_f	filter time constant
$\tau_{f/a}$	frequency-to-analog conversion time constant
τ_{GG}	gas generator time constant
τ_{T_4}	T_4 sensor time constant

DISTRIBUTION LIST

	No. of Copies

Commander IDDR&E
Pentagon, Room 3D 1089
Washington, D.C. 20310
Attn: Ltc. G. Kopesak   1

Defense Technical Information
Cameron Station, Building 5
Alexandria, VA 22314
Attn: DTIC-DDA   12

Office of the Deputy Chief of Staff for
   Research, Development, and Acquisition
Department of the Army
Washington, D.C. 20310
Attn: DAMA-ARP-P, Dr. V. Garber   1
Attn: Mr. John Hill, Room 3D424   1

U.S. Army R&D Group (Europe)
Box 15
F.P.O. New York 09510
Attn: Chief, Aeronautics Branch
Attn: Chief, Engineering Sciences

U.S. Army Research Office
P.O. Box 12211
Research Triangle Park, NC 27709
Attn: James J. Murray,   1
         Engineering Sciences Division

BMD Advanced Technology Center
P.O. Box 1500
Huntsville, AL 35807
Attn: J. Papadopoulos   1

Commander
USA Foreign Science and Technology Center
Federal Office Building
220 7th Street, Northeast
Charlottesville, VA 22901
Attn: DRXST-SD1   1

No. of
Copies

Director
Applied Technology Laboratory
Fort Eustis, VA 23604
Attn: George W. Fosdick, DAVDL-EA-SYA   1

Commander
USA Missile Research and Development Command
Redstone Arsenal, AL 35809
Attn: Redstone Scientific Information Center,   1
       DRSMI-RBD
Attn: DRDMI-TGC, William Griffith   1
Attn: DRDMI-TGC, J. C. Dunaway   1
Attn: DRCPM-TOE, Fred J. Cheplen   1

Commander
USA Mobility Equipment Research and
  Development Center
Fort Belvoir, VA 22060
Attn: Technical Library (Vault)   1
Attn: DRDME-EM, R. N. Ware   5

Commander
Edgewood Arsenal
Aberdeen Proving Ground, MD 21010
Attn: SAREA-MT-T, Mr. D. Patton   1

Commander
U.S. Army ARRADCOM
Dover, NJ 07801
Attn: SARPA-TS-S-#59   1
Attn: DRDAR-LCN-F, A. E. Schmidlin
Attn: DRDAR-LCW-E, Mr. J. Connor   1

Commander
Watervliet Arsenal
Watervliet Arsenal, NY 12189
Attn: SARWV-RDT-L   1

No. of
Copies

Commander
USA Tank Automotive Research and
  Development Command
Armor and Company Division, DRDTA-RKT
Building 215
Warren, MI 48090
Attn: T. Kozowyk   1
Attn: M. Steele   1

Commander
White Sands Missile Range, NM 88002
Attn: STEWS-AD-L, Technical Library   1

Commander
U.S. Army Armament Materiel Readiness Command
Rock Island, IL
Attn: DRSAR-RDG-T, Mr. R. Spencer   1
Attn: DRSAR-ASF   1

Office of Naval Research
Department of the Navy
Arlington, VA   22217
Attn: Stanley W. Doroff, Code 438   1
Attn: D. S. Siegel, Code 211   1

Department of the Navy
Research and Development Plans Division
Room 5D760, Pentagon
Washington, DC   20350
Attn: Benj R. Petrie, Jr.   1
        OP-987P4

Commander
Naval Air Development Center
Warminster, PA   18974
Attn: R. McGiboney,   30424   1
Attn: Code 8134, Lois Guise   1

DISTRIBUTION LIST (CONTD)

No. of
Copies

Naval Air Systems Command
Department of the Navy
Washington, DC   20360
Attn: Code AIR-52022A, J. Burns   1
Attn: Code AIR-52022E, D. Houck   1

Commander
Naval Ship Engineering Center
Philadelphia Division
Philadelphia, PA   19112
Attn: Code 6772, D. Keyser   1

Commander
Naval Surface Weapons Center
White Oak, MD   20910
Attn: Code 413, Clayton McKindra   1
Attn: Code WA-33, J. O'Steen   1

Commander
Naval Ordnance Station
Indianhead, MD   20640
Attn: Code 5123B, J. Morris   1

Naval Ship Research and Development Center
Bethesda, MD   20084
Attn: Code 1619, Mr. K. Reader   1

Naval Sea Systems Command
SEA0331H
Washington, DC   20362
Attn: A. Chaikin

Commander
Pacific Missile Range
Naval Missile Center
Point Mugu, CA   93042
Attn: Code 3123, Abe J. Garrett   1
Attn: Code 1243, A. Anderson   1

No. of
Copies

Commander
Naval Weapons Center
China Lake, CA 93555
Attn: Code 533, Library Division   1
Attn: Code 5536, Mr. M. D. Jacobson   1

Commander
Air Force Aero Propulsion Laboratory, AFSC
Wright-Patterson AFB, OH 45433
Attn: Lester Small 1TBC   1

Commander
Air Force Avionics Laboratory
Wright-Patterson AFB, OH 45433
Attn: RWN-2, Richard Jacobs   1

Director
Air Force Office of Scientific Research
1400 Wilson Boulevard
Arlington, VA 22209
Attn: NE, Mr. George Knausenberger   1

Commander
Air Force Flight Dynamics Laboratory
Wright-Patterson AFB, OH 45433
Attn: AFFDL/FGL, H. Snowball   1

Commander
Air Force Weapons Laboratory, AFSC
Kirtland AFB, NM 87117
Attn: SUL, Technical Library   1

Commander
Armament Development and Test Center
Eglin Air Force Base, FL 32542
Attn: ADTC (DLOSL), Technical Library   1

Air Force Flight Test Center
6510 ABG/SSD
Edwards AFB, CA 93523
Attn: Technical Library   1

No. of
Copies

Air Force Institute of Technology, AU
Wright-Patterson AFB, OH   45433
Attn: Library AFIT(LD),   1
        Building 640, Area B
Attn: AFIT(ENM), Milton E. Franke   1

Aerospace Medical Division
Brooks AFB, TX   78235
Attn: AMD/RDN, Cpt. G. James   1

Division of Reactor Research and Development
F-309 USERDA
Washington, DC   20545
Attn: Frank C. Legler   1

Oak Ridge National Laboratory
Central Research Library
Building 4500N, Room 175
P.O. Box X
Oak Ridge, TN   37830
Attn: E. Howard   1

Department of HEW
Public Health Service
National Institute of Health
Building 13, Room 3W-13
Bethesda, MD   20014
Attn: C. J. McCarthy   1

Department of Commerce
Bureau of East-West Trade
Office of Export Administration
Washington, D.C.   20230
Attn: Walter J. Rusnack   1

Scientific Library
U.S. Patent Office
Washington, D.C.   20231
Attn: Mrs. Cureton   1

No. of
Copies

Department of Commerce
National Bureau of Standards
Washington, D.C. 20234
Attn: Gustave Shapiro, 425.00   1

NASA Ames Research Center
Moffett Field, CA 94035
Attn: MS 244-13, Dean Chisel   1

NASA Langley Research Center
Hampton, VA 23665
Attn: MS 494, H. D. Garner   1
Attn: MS 494, R. R. Hellbaum   1
Attn: MS 185, Technical Library   1

NASA Lewis Research Center
21000 Brookpark Road
Cleveland, OH 44135
Attn: Vernon D. Gebben   1

NASA Scientific and Technical
  Information Facility
P.O. Box 8657
Baltimore/Washington International Airport,
  MD 21240
Attn: Acquisitions Branch   1

U.S. Army Electronics Research and
  Development Command
Attn: Robert S. Wiseman, DR., DRDEL-CT   1
Attn: PAO   1

Harry Diamond Laboratories
Attn: CO/TD/TSO   1
Attn: Chief, 00210   1
Attn: Chief, DIV 10000   1
Attn: Chief, DIV 20000   1
Attn: Chief, DIV 30000   1
Attn: Chief, DIV 40000   1
Attn: Chief, LAB 11000   1
Attn: Chief, LAB 13000   1

DISTRIBUTION LIST (CONCLUDED)

	No. of Copies
Harry Diamond Laboratories (Contd)	
Attn: Chief, LAB 15000	1
Attn: Chief, LAB 22000	1
Attn: Chief, LAB 21000	1
Attn: Chief, LAB 34000	1
Attn: Chief, LAB 36000	1
Attn: Chief, LAB 47000	
Attn: Chief, LAB 48000	
Attn: Record Copy, 81200	1
Attn: HDL Library, 81000	3
Attn: HDL Library, 81000 (Woodbridge)	1
Attn: Chairman, Editorial Committee	1
Attn: Technical Reports Branch, 81300	1
Attn: Legal Office, 97000	1
Attn: C. Lanham, 00210	1
Attn: B. Willis, 47400	1
Attn: Chief, 13400	1
Attn: J. Goto, 13400	5

APPENDIX A.-DUAL-CHANNEL FUEL CONTROL MODEL SIMULATION

The procedures and values used to perform the dual-channel fuel control model simulation are presented in the following paragraphs.

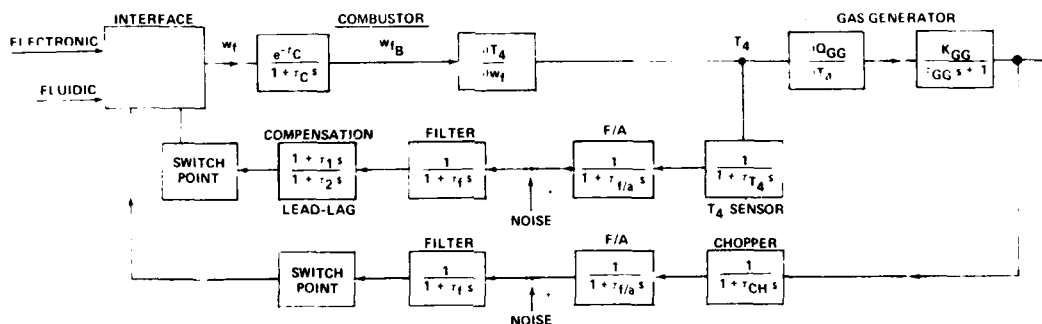The values listed in Table A-1 were used in the dynamic model in Figure A-1.


Figure A-1. Simplified dynamic model.

A preliminary evaluation of the engine model as presented in Figure A-2 showed that, for short time periods, the influences of the recuperator and the cross-coupling effects of the VTN and power turbine could be ignored. For purposes of determining the performance required of the failure detection circuits, the boxed-in parameters were used. The other parameters would have inhibited a failure condition from developing, or were weakly coupled to the gas generator inlet temperature and speed. The values in Table A-I correspond to hot day and an altitude environment of 3500 meters.

To conduct a simulation, the following parameters were set:

N_{switch} -   speed switch point

T_4 switch   - T_4 failure temperature switch point

T_4 rate   -   temperature ramp rate

τ_{filter} -   time constant of filter

TABLE A-I. PARAMETER VALUES USED IN SIMULATION.

	w_f	T_4	N_{GG}	N
Initialized Values	1200 lbm per hr	1800F	37,540 rpm	
Partials Affecting T_4	$\dfrac{\partial T_4}{\partial w_f}$ 4.31F per lbm per hr	$\dfrac{\partial T_4}{\partial N_{GG}}$ −0.0295F per rpm	$\dfrac{\partial T_4}{\partial \beta}$ 1.87F per deg	$\dfrac{\partial T_4}{\partial T_{3.5}}$ 0.891
Time Constants	$\tau_{T_4\text{sensor}}$ 0.025 s	τ_{fluidics} 0.005 s	$\tau_{\text{gas generator}}$ 0.221 s	
	$\tau_{\text{combustor}}$ 0.006 s	τ_{delay} 0.030 s	$\tau_{\text{recuperator}}$ 19.6 s	
Gas Generator Parameters	K_{GG} 338.2 rpm per ft-lbf			
	$\dfrac{\partial Q_{GG}}{\partial T_4}$ 0.0335 ft-lbf per deg	$\dfrac{\partial Q_{GG}}{\partial \beta}$ −0.0126 ft-lbf per deg		
Partials Affecting $T_{3.5}$	$\dfrac{\partial T_{3.5}}{\partial T_4}$ 0.568	$\dfrac{\partial T_{3.5}}{\partial N_{GG}}$ −0.011F per rpm	$\dfrac{\partial T_{3.5}}{\partial \beta}$ 4.7F per deg	
Variable Turbine Nozzle Angle	β −2.87 degrees			
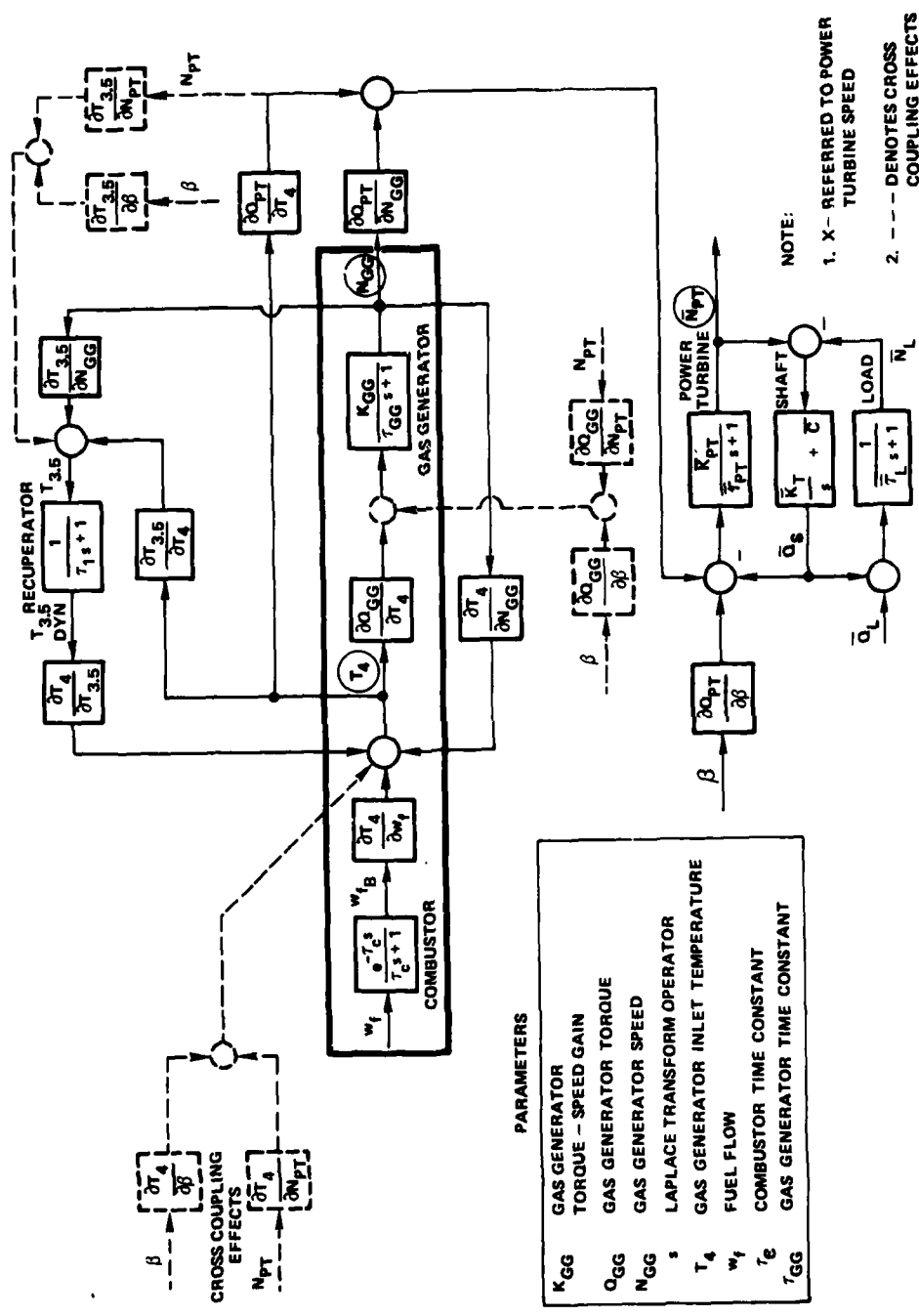
Figure A-2. Linearized model of GT601.

PARAMETERS

K_{GG}	GAS GENERATOR TORQUE – SPEED GAIN
Q_{GG}	GAS GENERATOR TORQUE
N_{GG}	GAS GENERATOR SPEED
s	LAPLACE TRANSFORM OPERATOR
T_4	GAS GENERATOR INLET TEMPERATURE
w_f	FUEL FLOW
τ_e	COMBUSTOR TIME CONSTANT
τ_{GG}	GAS GENERATOR TIME CONSTANT

NOTE:

1. $\overline{X}$ – REFERRED TO POWER TURBINE SPEED

2. – – – DENOTES CROSS COUPLING EFFECTS

43ART00151

71

The temperature and/or speed are then initialized and the lead/lag ratio of the compensator is set at values between one and 10, inclusive. A lead-lag ratio of one corresponds to no lead.

The settings listed in Table A-II were used for runs illustrated in Figures A-3 through A-13. For these simulations, the speed signal path was disconnected to produce a switch due only to overtemperature.

TABLE A-II. CONDITIONS OF SIMULATION RUNS WITH
SPEED SIGNAL PATH DISCONNECTED

Figure No.	T_4 switch	T_4 rate	filter	Lead/Lag ratio
	F	F per s	s	
A-3	1840	700	None	1
A-4	1840	100	None	1
A-5	1840	700	0.005	1
A-6	1840	100	0.005	1
A-7	1820	700	0.005	1
A-8	1820	100	0.005	1
A-9	1820	700	0.005	3
A-10	1820	700	0.005	10
A-11	1820	700	0.025	10
A-12	1820	700	0.025	3
A-13	1840	700	0.025	3
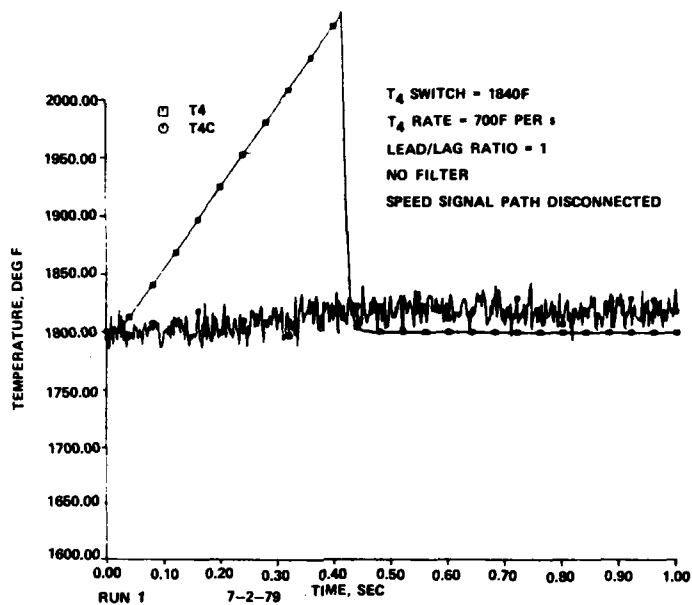
Figure A-3. Simulation run with speed signal
path disconnected.
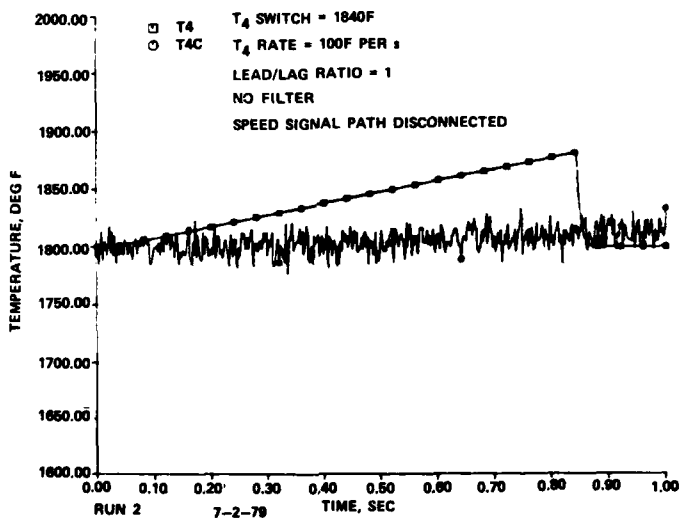
Figure A-4. Simulation run with speed signal
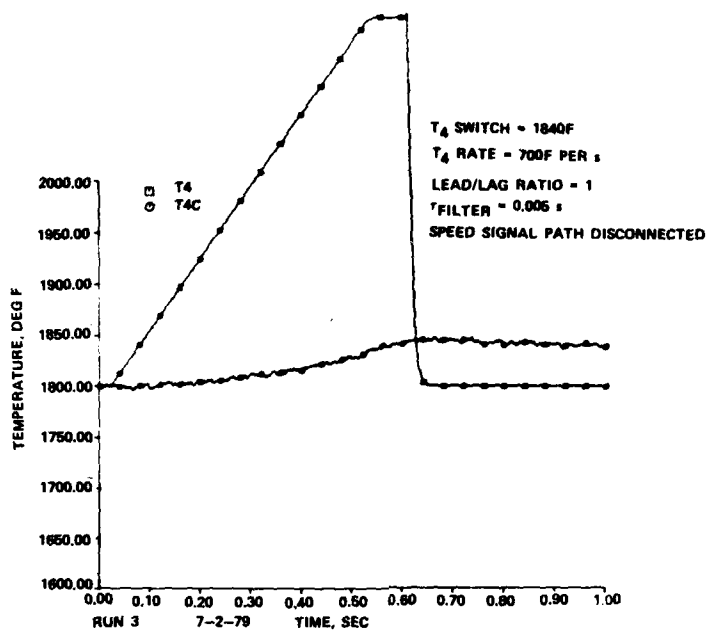path disconnected.

73

Figure A-5.   Simulation run with speed signal
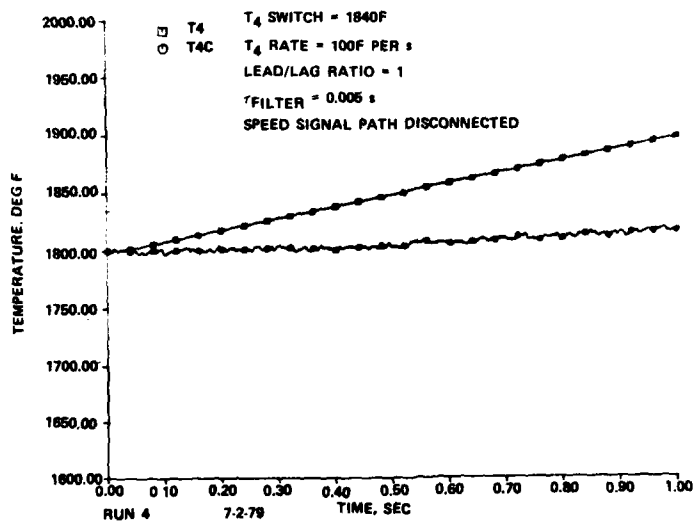   path disconnected.

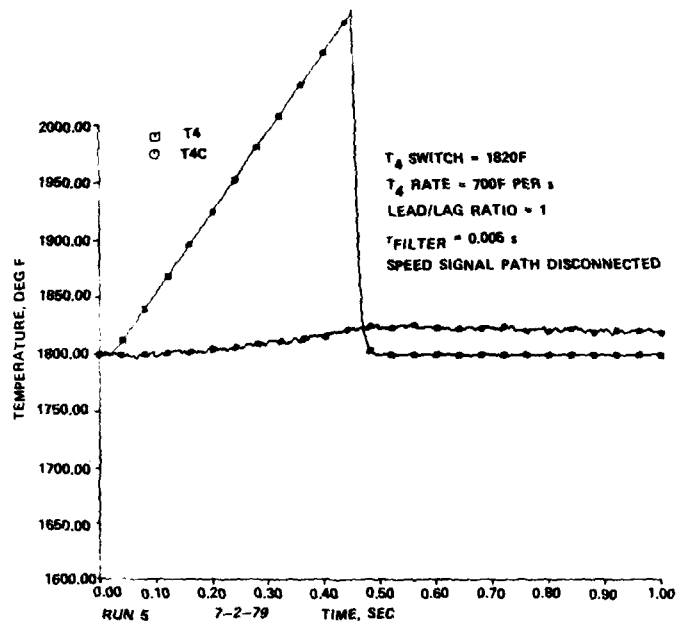Figure A-6.   Simulation run with speed signal
              path disconnected.

74

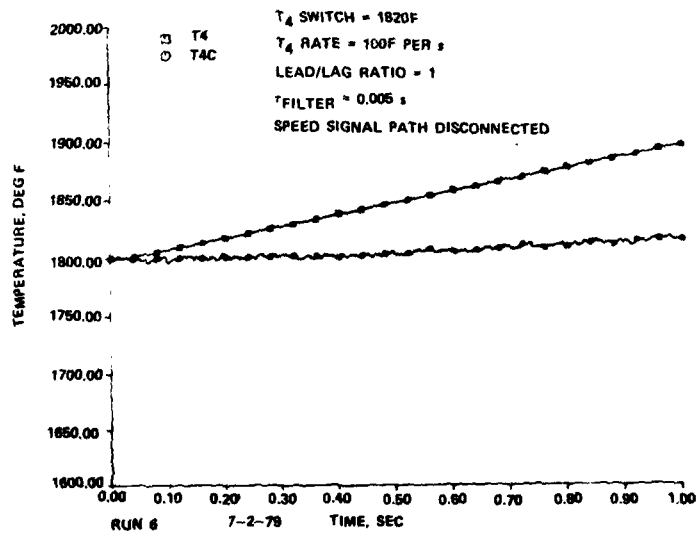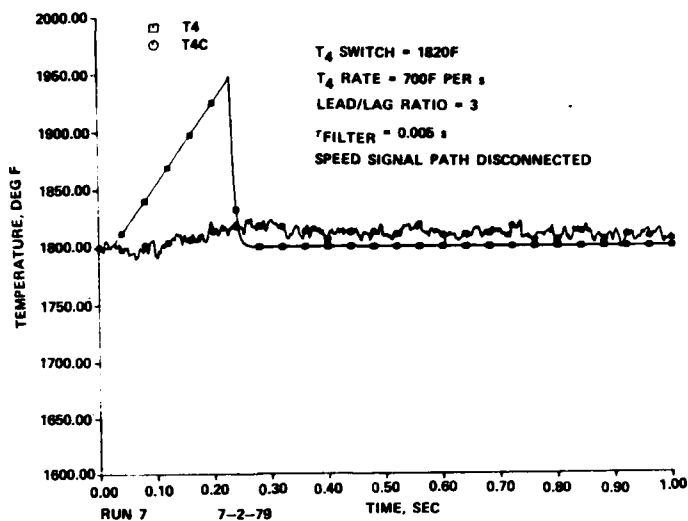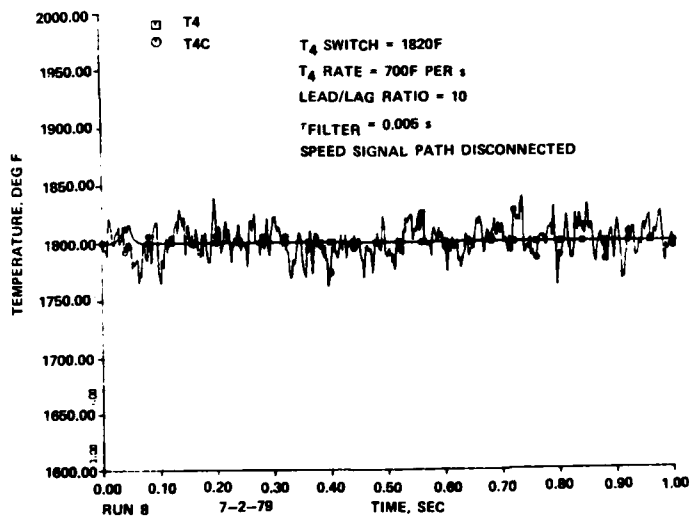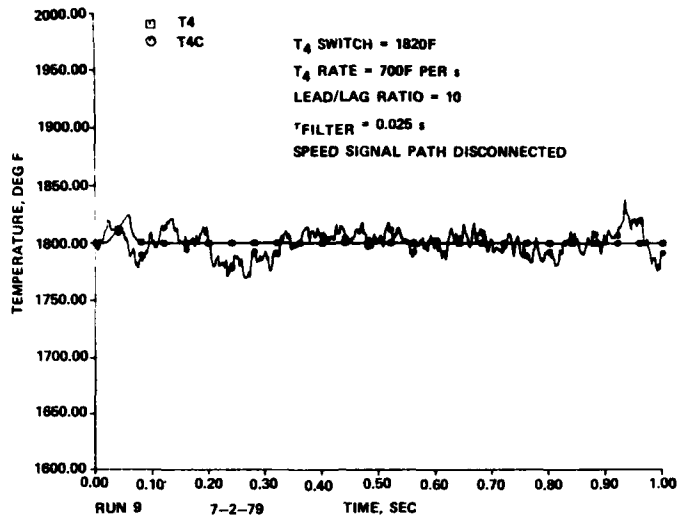Figure A-7. Simulation run with speed signal path disconnected.

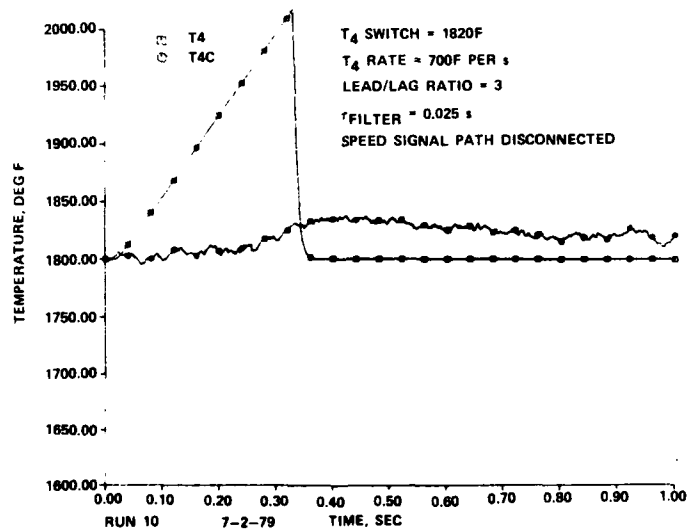Figure A-8. Simulation run with speed signal path disconnected.

75

Figure A-9. Simulation run with speed signal path disconnected.

Figure A-10. Simulation run with speed signal path disconnected.

76

Figure A-11.   Simulation run with speed signal
              path disconnected.

Figure A-12.   Simulation run with speed signal
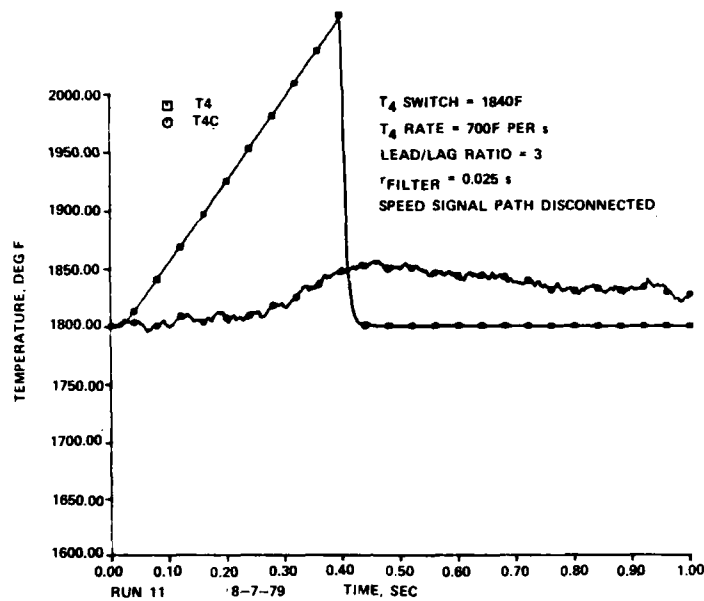   path disconnected.

77

Figure A-13.   Simulation run with speed signal
path disconnected.

Two runs were conducted with the temperature signal
path disconnected in order to produce failure conditions due
only to overspeed. Figures A-14 and A-15 present the traces
without a filter and with a filter (τ_{filter} = 0.025 s),
respectively. Other settings were as follows:

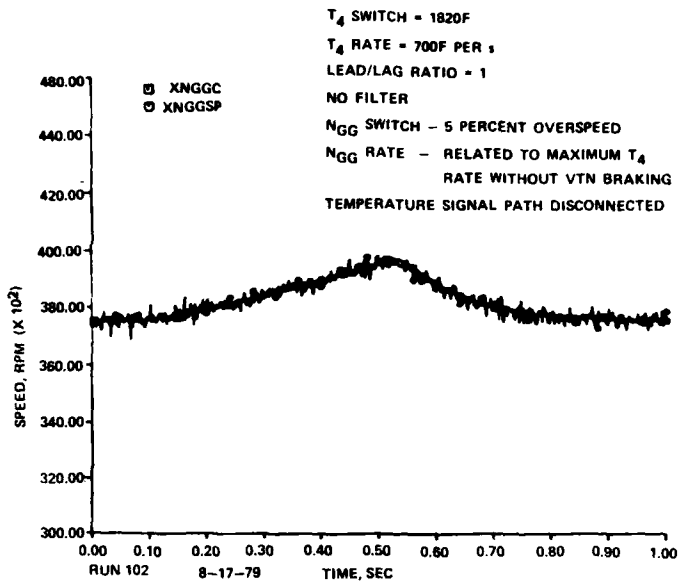| Parameter	Setting
T_4	1820F
T_4 rate	700F per s
Lead/lag ratio	1
N_{GG} switch	5 percent overspeed
N_{GG} rate	related to maximum T_4 rate without VTN braking

78

Figure A-14.   Simulation run with temperature signal
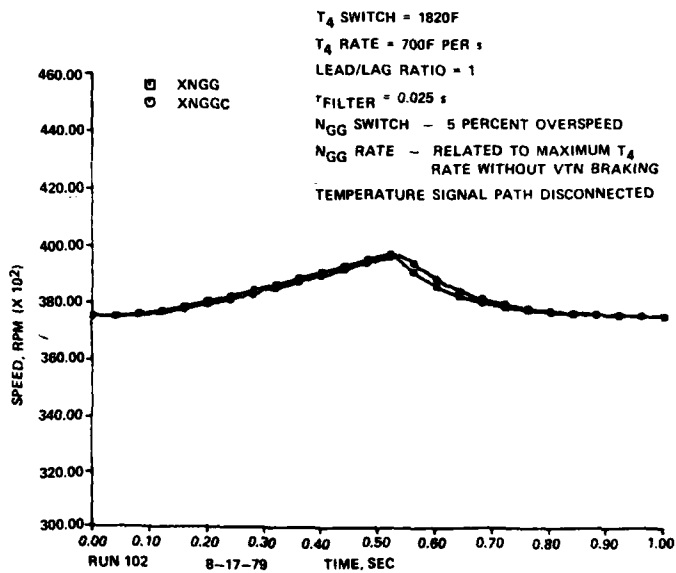   path disconnected (without filter).

Figure A-15.   Simulation run with temperature signal
              path disconnected (with filter).

79

A single run was conducted with a filter only on the speed path and with both speed and temperature signal channels connected to produce a switch (Figure A-16). Other settings were as follows:

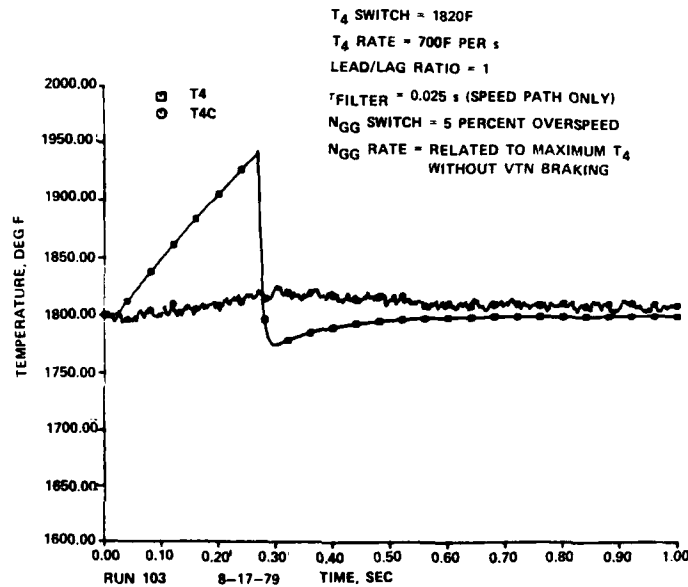| Parameter	Setting
T_4 switch	1820F
T_4 rate	700F per s
N_{GG} switch	5 percent overspeed
N_{GG} rate	related to maximum T_4 rate without VTN braking
Lead/lag ratio	1
τ_{filter}	0.025 s (speed path only)

Figure A-16. Simulation run with speed and temperature signals connected.